AGU PUBLICATIONS

Paleoceanography

RESEARCH ARTICLE

10.1002/2014PA002666

Key Points:
- Epsilon Nd response to CAS shoaling and Drake Passage deepening is modeled
- Model/data comparison of response to CAS shoaling favors a shallow Miocene AMOC
- Nd/circulation response to Drake Passage opening/deepening is nonlinear

Correspondence to:
P. L. Pfister,
pfister@climate.unibe.ch

Citation:
Pfister, P. L., T. F. Stocker, J. Rempfer, and S. P. Ritz (2014), Influence of the Central American Seaway and Drake Passage on ocean circulation and neodymium isotopes: A model study, *Paleoceanography*, *29*, doi:10.1002/2014PA002666.

Received 2 MAY 2014
Accepted 13 NOV 2014
Accepted article online 19 NOV 2014

Influence of the Central American Seaway and Drake Passage on ocean circulation and neodymium isotopes: A model study

Patrik L. Pfister[1,2], Thomas F. Stocker[1,2], Johannes Rempfer[1,2], and Stefan P. Ritz[1,2]

[1]Climate and Environmental Physics, Physics Institute, University of Bern, Bern, Switzerland, [2]Oeschger Centre for Climate Change Research, University of Bern, Bern, Switzerland

Abstract The sensitivity of the neodymium isotopic composition (ε_{Nd}) to tectonic rearrangements of seaways is investigated using an Earth System Model of Intermediate Complexity. The shoaling and closure of the Central American Seaway (CAS) is simulated, as well as the opening and deepening of Drake Passage (DP). Multiple series of equilibrium simulations with various intermediate depths are performed for both seaways, providing insight into ε_{Nd} and circulation responses to progressive throughflow evolutions. Furthermore, the sensitivity of these responses to the Atlantic Meridional Overturning Circulation (AMOC) and the neodymium boundary source is examined. Modeled ε_{Nd} changes are compared to sediment core and ferromanganese (Fe-Mn) crust data. The model results indicate that the North Atlantic ε_{Nd} response to the CAS shoaling is highly dependent on the AMOC state, i.e., on the AMOC strength before the shoaling to shallow depths (preclosure). Three scenarios based on different AMOC forcings are discussed, of which the model-data agreement favors a shallow preclosure (Miocene) AMOC (~6 Sv). The DP opening causes a rather complex circulation response, resulting in an initial South Atlantic ε_{Nd} decrease preceding a larger increase. This feature may be specific to our model setup, which induces a vigorous CAS throughflow that is strongly anticorrelated to the DP throughflow. In freshwater experiments following the DP deepening, ODP Site 1090 is mainly influenced by AMOC and DP throughflow changes, while ODP Site 689 is more strongly influenced by Southern Ocean Meridional Overturning Circulation and CAS throughflow changes. The boundary source uncertainty is largest for shallow seaways and at shallow sites.

1. Introduction

Changes in the global ocean circulation due to tectonic rearrangements of the Central American Seaway (CAS) and Drake Passage (DP) are recorded in the neodymium isotopic composition (ε_{Nd}), which can be extracted from sediment cores and ferromanganese (Fe-Mn) crusts. These changes and their climatic implications can also be studied using models. So far, model-data comparison was complicated by the fact that most models lack representations of certain water mass tracers such as ε_{Nd}, or by computational cost.

Here we present an ε_{Nd} sensitivity study of the CAS shoaling and closure, as well as the DP opening and deepening, using the Bern3D climate model. It is the first such study on the DP opening and deepening, including a model-data comparison of ε_{Nd} in the Southern Ocean. The CAS shoaling and closure have recently been investigated in a more highly resolved model [*Sepulchre et al.*, 2014], with a focus on ε_{Nd} in the Caribbean. In contrast, we analyze large-scale ε_{Nd} changes in the North Atlantic. Furthermore, the efficiency of our model does not only enable the simulation of a step-by-step shoaling but also a case-by-case analysis of the influence of the AMOC. This accounts for the large spread of possible AMOC responses inferred from earlier model studies (section 1.1); *Rempfer et al.* [2012a] have demonstrated that AMOC modifications have a substantial regional impact on seafloor ε_{Nd}, even without any seaway alterations. Due to the coarse model resolution, we cannot attempt a geologically realistic shape of the CAS and DP. Instead, the seaways are opened broadly and uniformly in modified modern bathymetries, to study the impact of varying throughflows in the relevant locations. Additional model experiments investigate the influence of the ε_{Nd} boundary source (see below), as well as the sensitivity of ε_{Nd} in the Southern Ocean to different circulation features.

ε_{Nd} is a quasi-conservative proxy of water mass mixing [*Frank*, 2002]. It is calculated from the isotopic concentrations ^{143}Nd (radiogenic) and ^{144}Nd as follows:

$$\varepsilon_{Nd} = \left(\frac{(^{143}Nd/^{144}Nd)_{sample}}{(^{143}Nd/^{144}Nd)_{std}} - 1 \right) \cdot 10^4 , \quad (1)$$

where the "Bulk Earth" standard ratio is 0.512638 [*Jacobsen and Wasserburg*, 1980]. Among other applications, ε_{Nd} is ideal for tracking interbasin exchange of water masses between the Atlantic and the Pacific [e.g., *Abouchami et al.*, 1999; *Burton et al.*, 1999; *Scher and Martin*, 2006; *Newkirk and Martin*, 2009], because of the distinctive signatures in these two basins. The older rocks of the North Atlantic continental crust are less radiogenic than the young volcanic material found in the North Pacific. Via neodymium (Nd) exchange at the continental margins (hereafter called "boundary source"), the water masses inherit this ε_{Nd} signature [*Lacan and Jeandel*, 2005; *Arsouze et al.*, 2007], and at distance from the margins essentially only change their intermediate and deep water Nd isotope compositions as a consequence of mixing with other water masses.

This paper is structured as follows. Previous research on the CAS shoaling and DP deepening is summarized in sections 1.1 and 1.2. Following the methods description of our model study (section 2), the results are presented and discussed in sections 3 to 6: An overview of circulation and ε_{Nd} in modified bathymetries is given in section 3, the CAS shoaling and DP deepening are presented separately in sections 4 and 5, and boundary source experiments are documented in section 6. Limitations of the study are discussed in section 7, followed by a summary and conclusions (section 8).

1.1. Shoaling and Closure of the Central American Seaway

Decreases in ε_{Nd} during the last roughly 13 million years were found in North Atlantic Fe-Mn crusts and Caribbean sediment cores and associated with the shoaling and closure of the Central American Seaway (CAS) [*Burton et al.*, 1997, 1999; *O'Nions et al.*, 1998; *Abouchami et al.*, 1999; *Frank et al.*, 1999; *Reynolds et al.*, 1999; *Newkirk and Martin*, 2009]. More specifically, the decreases have been related to a decreasing flow of radiogenic Pacific waters through the CAS [*Reynolds et al.*, 1999; *Newkirk and Martin*, 2009], or an intensification of North Atlantic Deep Water (NADW) formation in response to the CAS shoaling and closure, including increased contributions of very unradiogenic Labrador Sea Water [*Burton et al.*, 1997, 1999; *O'Nions et al.*, 1998]. However, the most recent decrease (~4 Ma to the present) may also at least in part be due to changes in weathering inputs related to the major intensification of Northern Hemispheric glaciation [*Frank et al.*, 1999; *Reynolds et al.*, 1999; *von Blanckenburg and Nägler*, 2001; *Muiños et al.*, 2008].

The timing of the geological evolution of the CAS (and the emerging Isthmus of Panama) is heavily debated based on geological, biological, and paleoceanographic evidence [*Molnar*, 2008; *Stone*, 2013]. While it is widely accepted that the CAS was fully closed by around 3 Ma, the recent geological studies by *Montes et al.* [2012a, 2012b] suggest that the seaway had already become as narrow as 200 km by the early Miocene, and that deep water communication between the Pacific and the Caribbean had ceased by 10 Ma or earlier. However, *Coates and Stallard* [2013] and others [*Stone*, 2013, and references therein] do not agree with this latter finding.

In model studies with modified modern or Miocene boundary conditions, an open CAS causes a net Pacific-to-Atlantic throughflow and weakens North Atlantic Deep Water (NADW) formation, thereby slowing the Atlantic Meridional Overturning Circulation (AMOC) [e.g., *Maier-Reimer et al.*, 1990]. In different models, the simulated CAS throughflows amount to 2–17 Sverdrup (Sv) and the AMOC responses range from a very slight decrease to a near shutdown, as compiled by *Sepulchre et al.* [2014]. (Note: The ancient counterpart of NADW is usually dubbed Northern Component Water (NCW). Because we are investigating modified modern bathymetries in this study, we utilize the term NADW for both counterparts. Similarly, we also utilize AABW (Antarctic Bottom Water) for Southern Ocean Deep Water.)

Among other impacts, the CAS shoaling and closure has also been related to a decrease in the North Pacific Overturning circulation [*Motoi et al.*, 2005; *von der Heydt and Dijkstra*, 2006; *Butzin et al.*, 2011], Northern Hemisphere glaciation [*Murdock et al.*, 1997; *Klocker et al.*, 2005; *Lunt et al.*, 2008], and a shoaling of the tropical thermocline [*Steph et al.*, 2010; *Zhang et al.*, 2012].

However, apart from the recent study by *Sepulchre et al.* [2014], none of the previous model studies have included Nd isotopes. *Sepulchre et al.* [2014] have calculated ε_{Nd} offline using the ocean circulation from a General Circulation Model (GCM) [*Arsouze et al.*, 2007] with a narrow CAS (400 km) in a similar location as

reconstructed by *Montes et al.* [2012b] for the Miocene. They have prescribed four different CAS depths and found a similar range in the simulated Caribbean ε_{Nd} average (at 500 m depth) as in Caribbean sediment data from *Newkirk and Martin* [2009].

1.2. Opening and Deepening of Drake Passage

Another major tectonic event that has been investigated by paleoceanographers for many decades is the opening of DP, separating South America from Antarctica. Its timing is even more uncertain compared to the CAS closure: estimates based on either tectonics or sediment parameters range from 6 to 50 Ma [*Eagles et al.*, 2006; *Barker et al.*, 2007, and references therein], with a majority lying in the middle to late Eocene or Oligocene epochs (i.e., between 41 and 23 Ma). Model experiments on the impact of DP on ocean circulation and climate have been conducted with various bathymetric settings: with idealized geometries [*Gill and Bryan*, 1971; *Toggweiler and Bjornsson*, 2000; *Smith et al.*, 2006], modified modern bathymetries [*Mikolajewicz et al.*, 1993; *Sijp and England*, 2004; *Sijp et al.*, 2009] and Eocene or Oligocene paleobathymetries [e.g., *Huber and Nof*, 2006; *Zhang et al.*, 2010; *Sijp et al.*, 2011].

The three most crucial impacts of the DP opening are closely linked: The onset of the Antarctic Circumpolar Current (ACC), its influence on Antarctic glaciation, and changes in the global meridional overturning circulation. For the ACC development, the opening of another seaway must be considered in addition to DP, namely, the Tasman Gateway separating Australia from Antarctica. It is not clear which of the two gateways was the last barrier for the ACC [*Barker et al.*, 2007; *Bijl et al.*, 2013]. While this causality is not crucial if one is mainly interested in the exchange of water masses between the Pacific and the Atlantic, it is important for the much discussed impact of these seaways on Antarctic glaciation [*Kennett*, 1977; *Toggweiler and Bjornsson*, 2000; *DeConto and Pollard*, 2003a, 2003b; *Barker et al.*, 2007; *Zhang et al.*, 2010; *Sijp et al.*, 2011; *Cristini et al.*, 2012; *Lefebvre et al.*, 2012; *Goldner et al.*, 2014].

The physical mechanism dubbed "Drake Passage effect" suggests that in the presence of an uninterrupted circumpolar Southern Ocean, a stronger ACC strengthens the AMOC, due to NADW-evoking Ekman suction in the Atlantic sector of the Southern Ocean [*Toggweiler and Samuels*, 1995]. In accordance with this, some model simulations with a closed DP or Eocene configuration show a weakened or even shut down AMOC [e.g., *Mikolajewicz et al.*, 1993; *Huber and Sloan*, 2001; *Sijp and England*, 2004]. However, the issue is complicated by the fact that the overturning is sensitive to changes in atmospheric greenhouse gas concentrations [*Heinemann*, 2009; *Lunt et al.*, 2010]. Model studies comparing bathymetries with an open and closed DP also find that the open passage causes a weakening of the Southern Ocean Meridional Overturning Circulation (SOMOC) [*Mikolajewicz et al.*, 1993; *Sijp and England*, 2004; *Sijp et al.*, 2009, 2011; *Cristini et al.*, 2012].

Although it is expected that the opening of DP has also affected the distribution of Nd isotopes, none of the above mentioned model studies have included these tracers. In sediment cores from the Atlantic sector of the Southern Ocean, *Scher and Martin* [2004, 2006] have found an ε_{Nd} increase in the middle Eocene. They have associated this increase with the inflow of radiogenic waters from the Pacific, i.e., with the opening of DP, and dated it to 41 Ma [*Scher and Martin*, 2006]. Following the increase, *Scher and Martin* [2008] have measured pronounced ε_{Nd} decreases in the Oligocene and Miocene and associated these mainly with enhanced NADW transport to the Southern Ocean.

2. Methods

2.1. Model Description

The Bern3D model is a coupled ocean-atmosphere model of intermediate complexity. Its three-dimensional ocean component is a frictional geostrophic balance model [e.g., *Müller et al.*, 2006], which is coupled to a single-layer energy and moisture balance model (EBM) [*Ritz et al.*, 2011]. The model geometry consists of 36 × 36 horizontal grid cells of equal area, and 32 logarithmically spaced depth layers with increasing thickness (from 39 m at the surface to 397 m at full depth of 5000 m). The ocean model's biogeochemical component is described in, e.g., *Tschumi et al.* [2008] and *Parekh et al.* [2008] and has recently been extended by the addition of Nd isotopes [*Rempfer et al.*, 2011], as described below. Due to its computational efficiency, the model is suitable for a wide range of paleoclimate studies [*Ritz et al.*, 2011, 2013; *Rempfer et al.*, 2012a; *Menviel et al.*, 2012; *Roth and Joos*, 2013] and sensitivity studies [*Parekh et al.*, 2008; *Tschumi et al.*, 2008; *Ritz et al.*, 2011; *Rempfer et al.*, 2011, 2012b].

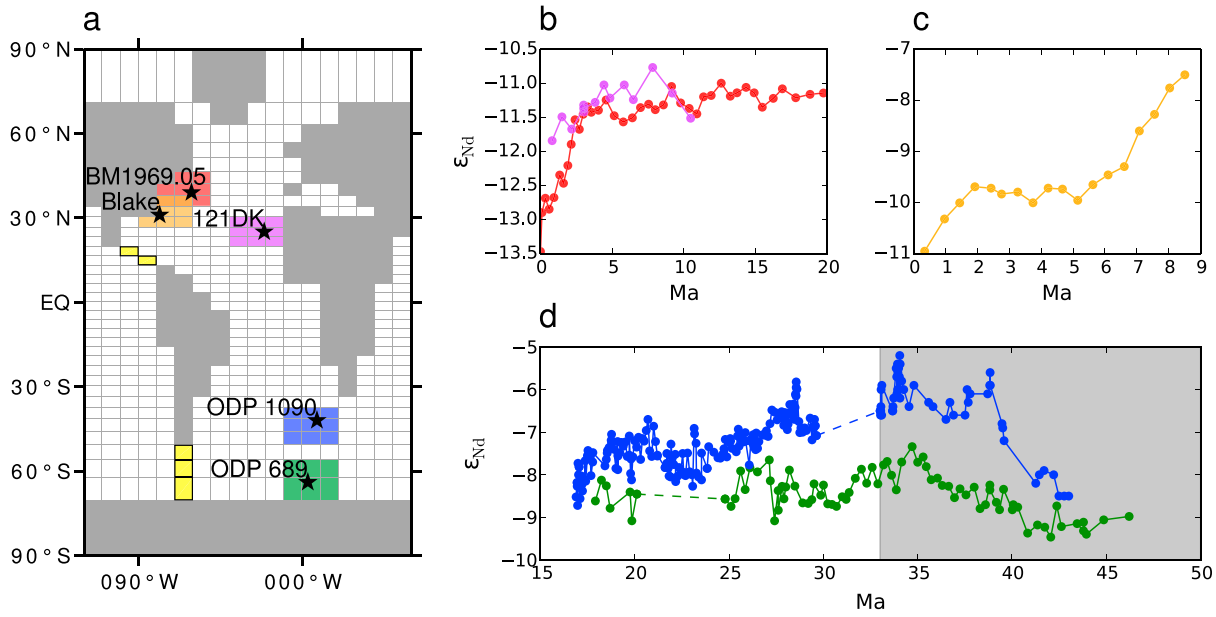

Figure 1. (a) Locations of sediment cores and Fe-Mn crusts (labeled stars) on the Bern3D model grid and corresponding regions over which the modeled ε_{Nd} is averaged for model-data comparison (colors). Highlighted in yellow are cells that are modified in the CAS shoaling and Drake Passage deepening experiments. Data of ε_{Nd} from these sediment cores or Fe-Mn crusts, colors corresponding to the regions in Figure 1a. (b) Sites BM1969.05 [*Burton et al.*, 1999] (red) and 121DK [*Abouchami et al.*, 1999] (purple); (c) "Blake" (Site BM1963.897) [*Reynolds et al.*, 1999]; (d) ODP Sites 1090 (blue) and 689 (green) [*Scher and Martin*, 2004, 2006, 2008]. The data related to the DP opening and deepening by *Scher and Martin* [2006] are shown with a grey background. Additional data from *Scher and Martin* [2004, 2008] are shown with a white background.

Rempfer et al. [2011] incorporated Nd isotopes into the Bern3D model, the modeled modern ε_{Nd} distribution is in reasonable agreement with measurements. In contrast to the approach by *Arsouze et al.* [2007], the ^{143}Nd and ^{144}Nd concentrations are treated separately. In addition to Nd dust and river sources, a constant boundary source is prescribed at depths between 0 and 3000 m. The only Nd sink in the model is the Nd removal by sinking particles, parameterized using the "reversible scavenging" approach [*Bertram and Elderfield*, 1993; *Rempfer et al.*, 2011].

2.2. Gateway Modifications

For this study, we alter the DP and Panama regions in the Bern3D modern bathymetry. Grid cells which are modified are marked in yellow in Figure 1. For the CAS, an opening width of two cells is selected to avoid computations on a single-gridbox level. For DP, the three cells that are open in the model's modern bathymetry are chosen. We do not attempt to create more realistic bathymetric shapes due to the coarse resolution of our model. CAS and DP openings merely serve as Atlantic-to-Pacific connections providing throughflows in roughly the relevant locations, the impact of which can be studied. The throughflow strength is modified by varying the seaway depth as described below.

An overview of all model experiments is given in Table 1, including explanations of the acronyms. The CAS cells are opened uniformly, layer by layer, starting from the modern bathymetry. The maximum opening depth is determined by the depth of neighboring grid cells and amounts to roughly 2100 m (22 layers). For the modern bathymetry (CTRL) and each of the 22 bathymetries with different CAS depths (CSTD1-22), separate model spin-ups are carried out. Each spin-up is run for 30,000 model years to ensure equilibration of the ε_{Nd} distribution. Tectonic rearrangements such as the CAS shoaling are slow enough to maintain oceanic equilibrium; therefore, these 23 simulations (starting with the deepest CAS) qualitatively represent a CAS shoaling from a deep seaway to a fully closed one. This series of spin-ups is labeled CSTD in the remainder of this paper.

Similarly, the DP cells are opened uniformly, starting with a fully closed DP and a relatively (1300 m) deep CAS (EOCTRL). This CAS depth was chosen as it is the shallowest depth for which the model does not increase boundary drag. It is kept constant for all DP opening depths. DP is gradually opened up to a depth of roughly 2500 m (24 layers). This series of 25 simulations (EOCTRL-DSTD24) is summarizingly labeled DSTD.

Table 1. Overview of Model Experiments[a]

	Control Simulations
CTRL	*Modern **control** run*
EOCTRL	*"Pseudo-**Eo**cene" **control** run* (with closed DP and ~1300 m deep CAS)
	Central American Seaway (CAS) Experiment Series
CSTD	*CAS shoaling and closure with **St**andar**d** APF*[b] 23 model runs, representing shoaling of the CAS from ~2100 m depth (CSTD22) to closed (CTRL)
CN10	like CSTD but with ***N**orth APF reduced to **0.10** Sv*
CB10	***B**oth North and South APF reduced to **0.10** Sv*
CN00	***N**orth APF reduced to **0.00** Sv*
CB00	***B**oth North and South APF reduced to **0.00** Sv*
CSTDa	like CSTD but with *CAS boundary source modification **a*** (no seafloor boundary source in the Caribbean)
CSTDb	*CAS boundary source modification **b*** (no boundary source in the Caribbean)
	Drake Passage (DP) Experiment Series
DSTD	***D**P opening and deepening with **St**andar**d** APF* 25 model runs, representing deepening of DP from closed (EOCTRL) to ~2500 m depth (DSTD24)
DN10-DB00	like DSTD but with APF modifications as in CN10-CB00 (see above)
DSTDa	like DSTD but with *DP boundary source modification **a*** (most unradiogenic Antarctic boundary source cell is turned off)
DSTDb	*DP boundary source modification **b*** (no Antarctic Boundary Source)
DSTD24fw	*10 freshwater (**fw**) experiments starting from* DSTD24, with a negative fw input of −0.02 to −0.20 Sv in the North Atlantic (section 2.4)
DN1024fw-DB0024fw	like DSTD24fw, but with APF modifications as in CN10-CB00 (see above)

[a]All acronyms (except the control simulations) correspond to a series of multiple simulations, e.g., CSTD consists of CTRL and CSTD1–CSTD22, where the number suffix denotes the depth of the Central American Seaway (CAS) in model layers.
[b]Here APF is short for Atlantic-to-Pacific freshwater flux (section 2.3).

While the introduction of an Eocene or Oligocene paleobathymetry (accompanied by modified climate forcings and Nd boundary conditions) would be beyond the scope of this study, including an open CAS along with a shallow or closed DP qualitatively represents the seaway connections between the Atlantic and the Pacific during these epochs.

2.3. AMOC Forcing

In the model's modern control, an Atlantic-to-Pacific freshwater flux [*Zaucker et al.*, 1994] is applied to compensate for its lack of a dynamical atmosphere. The flux strength, which is set to 0.17 Sv from the South Atlantic to the South Pacific and 0.17 Sv from the North Atlantic to the North Pacific [*Ritz et al.*, 2011], is an effective tuning parameter for AMOC strength. We will therefore use the shorthand term "AMOC forcing" synonymously with "Atlantic-to-Pacific freshwater flux strength." Note that the AMOC forcing does not prescribe the AMOC, it is merely one of many factors influencing the model's salinity balance; therefore, the AMOC strength may still be changed by other such factors, e.g., the CAS depth. Because the northern part (N) of the AMOC forcing has a stronger impact than the southern part (S), we select the following modifications to probe the AMOC sensitivity of the seaway experiments: reducing N to 0.10 Sv (CN10/DN10), or both N and S to 0.10 Sv (CB10/DB10); reducing N to zero (CN00/DN00), or both to zero (CB00/DB00). Here all of the acronyms in brackets do not correspond to single simulations but to series of spin-ups (like CSTD/DSTD); see Table 1.

Table 2. Depths of the Sites That Are Used for Model-Data Comparison and References to the Corresponding Data

Site	Depth	Reference
Blake (BM1963.897)	850 m	*Reynolds et al.* [1999]
BM1969.05	1850 m	*Burton et al.* [1999]
121DK	2000 m	*Abouchami et al.* [1999]
ODP 1090	3700 m	*Scher and Martin* [2006, 2008]
ODP 689	1600 m	*Scher and Martin* [2004, 2006]

2.4. Freshwater Experiments

To test the impacts of a stronger AMOC increase when DP is deep (24 layers), additional freshwater experiments are conducted in this bathymetry (DSTD24). Starting from DSTD24, 10 simulations are run with a constant negative freshwater flux in the North Atlantic, amounting to −0.02

to −0.2 /Sv (increments of −0.02 Sv, DSTD24fw01-DSTD24fw10). The simulations are run for 5000 years, which is enough for the ocean circulation to equilibrate. To avoid proximity to the CAS, the freshwater flux is only prescribed north of the Mediterranean, i.e., in latitudes of roughly 40°N–70°N. The flux is not compensated to avoid a secondary forcing influence of the compensating flux [*Stocker et al.*, 2007]. The freshwater experiments are repeated with the different AMOC forcings (i.e., starting from DN1024, DB1024, DN0024, and DB0024).

2.5. Boundary Source Modifications

We modify the Nd boundary source in relevant regions to check the robustness of the results with respect to boundary source uncertainties. Model runs with these modifications are only performed for the standard AMOC forcing (CSTD, DSTD). In the CAS experiments, we apply two different modifications in the Caribbean region. First, only the boundary source of Caribbean cells that are not land cells in the modern bathymetry is set to zero (CSTDa). Second, also the boundary source of the continental margin of the Caribbean, as well as the CAS cells, is set to zero (CSTDb). The latter modification is quite drastic, as most of the continental margin is only one land cell wide; therefore, the boundary source in the Pacific is also affected by these cells. In the DP experiments, two modifications to the Antarctic boundary source are applied: first, only the single most negative ($\varepsilon_{Nd} \approx -40$) boundary source cell is set to zero (DSTDa); second, the entire Antarctic boundary source is removed (DSTDb). These sensitivity experiments are especially relevant, considering that boundary exchange with the Antarctic continent is hardly detectable in the present-day water column even closest to Antarctica [*Stichel et al.*, 2012]. In the modern Caribbean, there is recent evidence for significant boundary exchange in the deep water [*Osborne et al.*, 2014] but with a less radiogenic signature than the extrapolated map by *Jeandel et al.* [2007] and model studies based on this map suggest [e.g., *Rempfer et al.*, 2011; *Sepulchre et al.*, 2014; this study].

2.6. Model-Data Comparison

Figure 1a shows the locations of sediment cores and Fe-Mn crusts from which records are used for comparison with the model results. The published records are shown in Figures 1b–1d: from Sites 121DK [*Abouchami et al.*, 1999] and BM1969.05 [*Burton et al.*, 1999] (Figure 1b), Site BM1963.897 ("Blake," Figure 1c), and Ocean Drilling Program (ODP) Sites 689 and 1090 [*Scher and Martin*, 2006] (Figure 1d). From *Abouchami et al.* [1999], only one record is chosen for the comparison, because the two cores they examined are relatively close with respect to the coarse model resolution. Site 121DK was selected over Site 65GTV because we are more interested in East Atlantic NADW than Mediterranean Outflow Water. Similarly, *Burton et al.* [1999] present data from two even closer sites (BM1969.05 and ALV539), from which the longer record from BM1969.05 is chosen. In Figure 1d, the data with a grey background are probably related to the DP opening and deepening [*Scher and Martin*, 2006] and are compared with the corresponding model simulations (section 5.3); the data with a white background are probably related to increased NADW export [*Scher and Martin*, 2008].

From the model output, nonweighted averages of ε_{Nd} values in a 3×3×3 cell region around the core sites are computed for comparison with the data. The cell that contains the estimated depth of the corresponding Fe-Mn crust or sediment core is chosen as the vertical center, where Eocene paleodepths according to *Scher and Martin* [2006] are used in case of the sediment cores (Table 2). The horizontal averaging regions are shown in Figure 1a, in colors corresponding to Figures 1b–1d.

3. Circulation and Seafloor ε_{Nd} in Modified Bathymetries

Before the circulation and ε_{Nd} responses to intermediate CAS and DP depths are discussed (sections 4 and 5), a comparison of closed versus deep gateways is presented here. Figure 2 shows the barotropic ocean circulation and seafloor ε_{Nd} in four different bathymetries. Figures 2a–2d compare the modern bathymetry (CTRL) to a bathymetry with a 1300 m deep CAS (CSTD16). The CTRL circulation (Figure 2a) shows a reasonable representation of the modern global gyre circulation, but a very weak ACC (∼ 40 Sv) compared to observations (e.g., *Cunningham et al.* [2003], report a modern ACC of 134 Sv).

In CSTD16 (Figure 2c), the gyre circulation is not substantially changed (Figure 2c), apart from the weakening of the Atlantic Subpolar Gyre, which is directly related to the slower AMOC (section 4.1). Although the stream function values in the Southern Hemisphere are shifted, the DP throughflow is not notably strengthened (<1 Sv). The CAS throughflow of roughly 9 Sv incorporates parts of the South Pacific and North Atlantic subtropical gyres into an interhemispheric branch of the ACC, strengthening the western boundary current along eastern South America. This also creates a direct flow connection between the CAS and

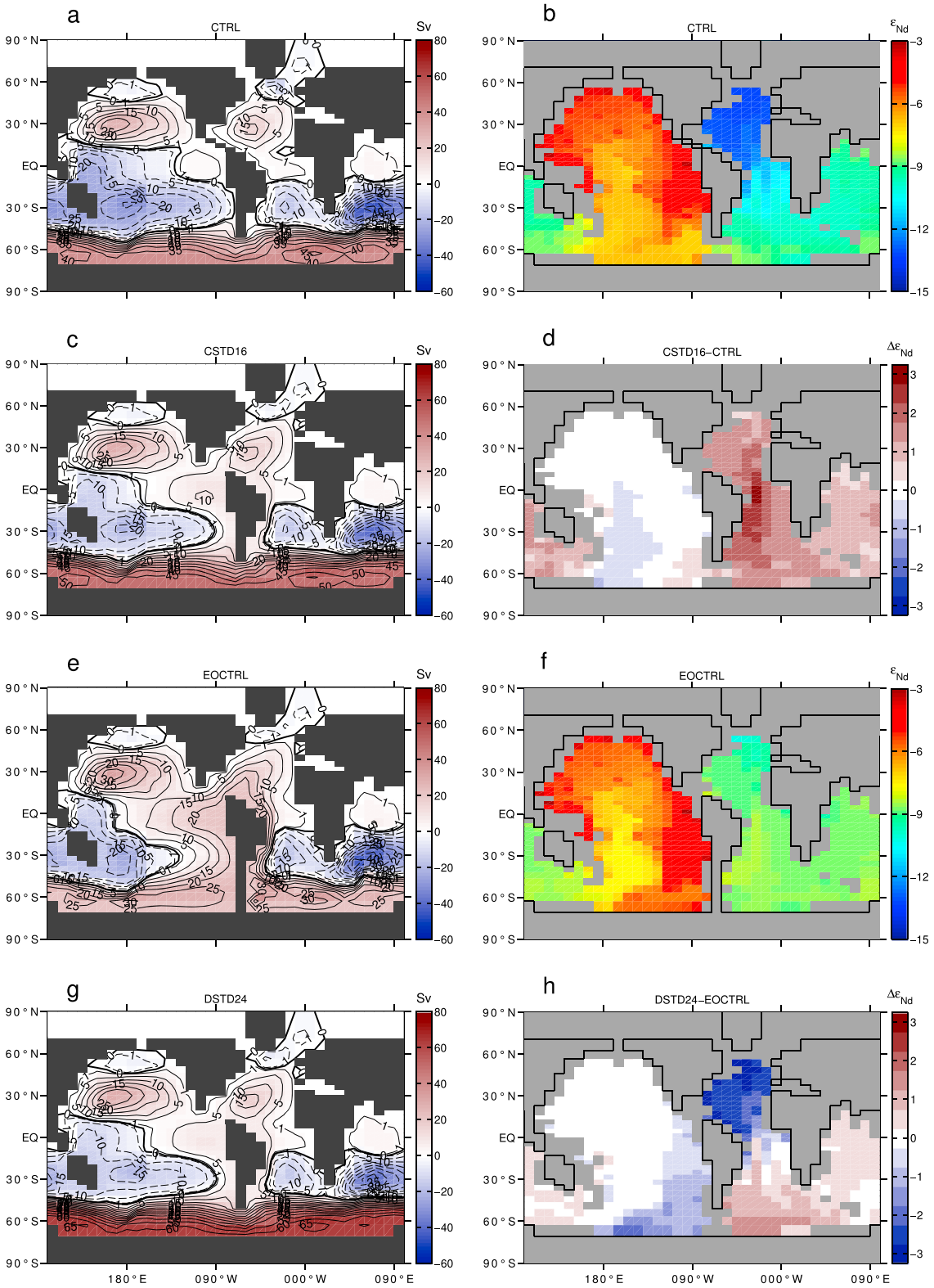

Figure 2. Barotropic ocean circulation and seafloor ε_{Nd} distribution in four different bathymetries: (a, b) modern (CNTRL); (c, d) open CAS at ~1300 m depth (CSTD16); (e, f) open CAS with closed Drake Passage (EOCTRL); and (e, h) open CAS with ~2500 m deep Drake Passage (DSTD24). While the absolute ε_{Nd} signatures are shown for CTRL (Figure 2b) and EOCTRL (Figure 2f), anomalies are displayed for CSTD16 (Figure 2d) and DSTD24 (Figure 2h). Only cells that have no boundary source (i.e., a depth of 3000 m or greater) are shown, shallower cells are shaded in grey. Circulation strength is shown in Sverdrup (10^6 m^3/s), and flow is clockwise around positive values.

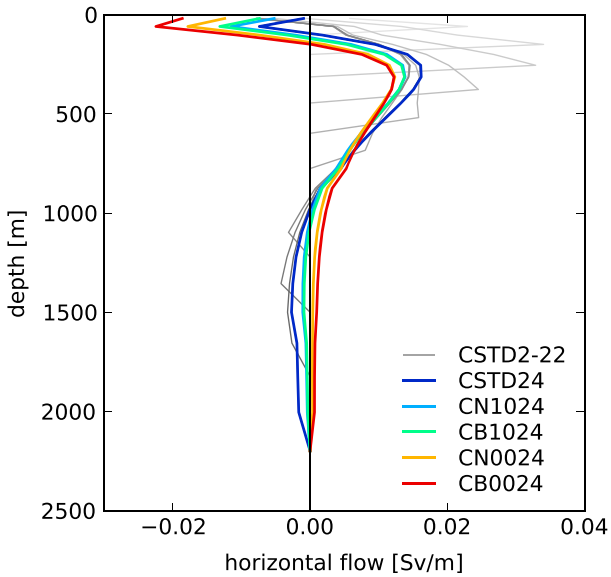

Figure 3. Depth profiles of the horizontal circulation through the CAS (positive eastward) in five model experiments with different AMOC forcings. CSTD and CB00 are the experiments with the strongest and weakest AMOC, respectively (Table 1). The throughflow profiles in the bathymetry with the deepest CAS (~ 2100 m) are shown in colors, e.g., CSTD24 for CSTD. Only for CSTD, the profiles in bathymetries with intermediate opening depths (CSTD2-22) are also shown, in shades of grey. Circulation strength is plotted in Sverdrup (10^6 m^3/s) per meter.

the North Atlantic. In models with a more realistic Caribbean bathymetry, this connection is weaker and limited to the surface [e.g., *Sepulchre et al.*, 2014]. However, in addition to this weaker direct flow, Pacific water masses passing the CAS can also be transported into the North Atlantic indirectly via gyre circulation.

The CTRL seafloor ε_{Nd} shown in Figure 2b is in reasonable agreement with observations [*Rempfer et al.*, 2011, Figure 9]. The differences in ε_{Nd} between CSTD16 and CTRL are shown in Figure 2d. The open CAS increases seafloor ε_{Nd} in the Atlantic and, to a smaller extent, in the Indian Ocean. Note that the increase in the Indian Ocean and the Atlantic sector of the Southern Ocean is probably overestimated, due to the too weak influence of the ACC in this region. However, the increase in the Atlantic sector is also amplified by the reduced inflow of unradiogenic NADW [*Rempfer et al.*, 2012a]. In the Pacific, seafloor ε_{Nd} is only slightly less radiogenic in CSTD16 than in CTRL. This is because the Pacific is a large reservoir of radiogenic Nd, such that the increased transport of such Nd to the Atlantic only has a minor effect on the Pacific ε_{Nd} signature; even less so at the seafloor, because the transport predominantly occurs at intermediate water depths.

Figures 2e–2h compare the first (EOCTRL) and last (DSTD24) bathymetry of the DP opening experiments (Table 1). The EOCTRL circulation (Figure 2e) features a vigorous (~22 Sv) eastward CAS throughflow originating in the Southern Ocean. As detailed in section 7, this throughflow is stronger than in other models, especially than in those with Eocene boundary conditions [e.g., *Heinemann*, 2009; *Sijp et al.*, 2011]. In DSTD24 (Figure 2c), the CAS throughflow is weakened compared to EOCTRL, and similar to CSTD16. The only difference between DSTD24 and CSTD16 is the uniform shape of the DP in DSTD24, which enables a stronger ACC (57 Sv, as opposed to 40 Sv).

The EOCTRL seafloor ε_{Nd} distribution (Figure 2f) is similar to the CTRL distribution (Figure 2b) in most regions. The most notable difference is the Atlantic ε_{Nd}, which is more radiogenic in EOCTRL, especially in the North. The well-mixed Atlantic signature is due to the strong CAS throughflow (Figure 2e). Furthermore, ε_{Nd} in the Indian Ocean is more homogeneous because less unradiogenic Nd is mixed into the western Indian Ocean. When DP is opened to great depth (DSTD24, Figure 2h), the ACC causes a more uniform ε_{Nd} signature in the Southern Ocean. This results in an ε_{Nd} increase in the South Atlantic, the Indian Ocean, and most markedly the Atlantic sector of the Southern Ocean, but a decrease in the Pacific sector. Additionally, the North Atlantic ε_{Nd} becomes less radiogenic due to the weakened CAS throughflow with an open DP.

4. Shoaling and Closure of the Central American Seaway

4.1. Circulation Changes

To better understand the ε_{Nd} response to a CAS opening, it is instructive to first describe the depth profile of the CAS throughflow, depending on CAS depth and AMOC forcing (section 2.3). Figure 3 shows the depth profile of the horizontal circulation through CAS in various experiments. The circulation for a 2100 m deep CAS is shown for each AMOC forcing (colors). In all but the two weakest AMOC cases CN00 and CB00 (in which the AMOC amounts to less than 3 Sv with a deep CAS), a westward transport of NADW into the Pacific is found below 1000 m depth. This feature has also been found in earlier EMIC simulations [*Nisancioglu et al.*, 2003; *Schneider and Schmittner*, 2006], but not in GCM simulations [e.g., *Lunt et al.*, 2008; *Sepulchre et al.*,

2014]. On the other hand, the GCM simulations feature a wind-driven westward surface flow that is not present in the mentioned EMIC studies, but found in the Bern3D circulation, due to the wind stress forcing in this region. In all experiments shown in Figure 3, however, the net throughflow is eastward, i.e., from the Pacific to the Atlantic. Consistent with the 2–17 Sv range found in previous model studies [*Sepulchre et al.*, 2014, and references therein], it amounts to 0–10 Sv, as seen in Figure 4a. Only in the simulations with the shallowest CAS and weakest Atlantic-to-Pacific freshwater flux (i.e., smallest interbasin salinity gradient), the wind-driven surface flow prevails, resulting in a net Atlantic-to-Pacific flow. This can be seen in Figure 4a as a negative CAS throughflow in the four shallowest openings of CN00 and CB00. Overall, the simulated depth profile shown in Figure 3 is in qualitative agreement with the profile found by *Butzin et al.* [2011] in a Miocene bathymetry of a more finely resolved EMIC (compare their Figure 10).

Figure 4 shows the CAS throughflow, AMOC strength and ε_{Nd} response in the five CAS shoaling experiments with different AMOC forcings. The above described NADW flow into the Pacific is also visible in Figure 4a as a decrease in net CAS throughflow for seaway depths larger than 1000 m, if the AMOC forcing is sufficiently strong (i.e., in CSTD, CN10, and CB10). Interestingly, the wide spread of AMOC strengths in the modern bathymetry is narrowed down to three AMOC states (of roughly 3, 6, and 9 Sv) when the CAS depth is about 400 m or deeper (Figure 4b). In other words, the AMOC difference between CN10 and CB10, and between CN00 and CB00, vanishes for a deep CAS. This implies that the importance of the southern part of the Atlantic-to-Pacific freshwater flux is diminished when direct water mass exchange between the two basins is allowed north of the equator. Furthermore, the net flow through the deepest CAS (2100 m) amounts to roughly 7.5 Sv, independent of AMOC strength. We infer that, for a deep CAS, the equilibrium between atmospheric freshwater flux and CAS throughflow is not regulated by the net throughflow strength, but mainly by the intensity of the AMOC.

In all experiments except CB00, the AMOC increase in response to a CAS shoaling and closure amounts to about 6–8 Sv (Figure 4b). This absolute range is small, but the relative increase compared to the deep-CAS AMOC strength ranges from roughly 75% (CSTD) to 200% (CN00). The latter increase is similar to GCM simulations that show a very sluggish AMOC prior to the CAS closure [*Sepulchre et al.*, 2014], although the AMOC in the modern bathymetry is too weak in CN00 ($\sim$ 9 Sv). Experiment CB00 is highly unrealistic, as it features a completely shut down AMOC in the modern bathymetry. It is notable, however, how much the CAS throughflow and ε_{Nd} responses to shallow CAS modifications differ in the absence of a modern AMOC (Figures 4a–4e, CB00).

4.2. The ε_{Nd} Response in the North Atlantic

Now, we look at the modeled ε_{Nd} response in the Western and Eastern North Atlantic (Figures 4c–4e). The largest ε_{Nd} range is found around the shallow Blake site (Figure 4c). This site's ε_{Nd} evolution is dominated by a pronounced ε_{Nd} decrease. This is because the eastward flow through CAS at $\sim$100–1000 m depth (Figure 3) decreases as CAS shoals, transporting less Pacific water to Blake. The ε_{Nd} decrease starts at a CAS depth of $\sim$900 m in CN00 and CB00, and $\sim$700 m in CN10, CB10 and CSTD. This difference is due to the delayed CAS throughflow decrease in CN10, CB10, and CSTD (Figure 4a and section 4.1).

With an intermediate to normal AMOC forcing, the ε_{Nd} decrease around Blake stops at $\sim$ 250 m depth and is followed by an increase (Figure 4c: CN10, CB10, and CSTD). This is because the AMOC does not only become stronger but also less shallow as the CAS shoals. Figure 5 compares the circulation in CN1027 and CN1032, the first and last experiments of this Blake ε_{Nd} increase (highlighted by red circles in Figure 4c). In the horizontal circulation averaged between $\sim$500 m and $\sim$1000 m depth, we see a southward flow in the central Atlantic in CN1027 (Figure 5a), but a northward flow in CN1032 (Figure 5b). This explains the ε_{Nd} increase at Blake (marked by a star), which shifts from receiving North Atlantic waters toward receiving more radiogenic waters from the South Atlantic and Indian Oceans. This is directly related to the fact that the intensifying AMOC also becomes deeper: in CN1027 (Figure 5c), the depth region shown in Figures 5a and 5b (blue band) is mainly influenced by the southward flow of NADW, while in CN1032 (Figure 5d), the NADW flow is deeper and this depth region is mainly influenced by the subsurface return flow.

With a low AMOC forcing, the ε_{Nd} decrease continues until the CAS is fully closed (Figure 4c: CN00). No ε_{Nd} increase occurs because the AMOC does not increase beyond 9 Sv, the minimum value that was needed in CN10 and CB10 to cause an ε_{Nd} increase (Figures 4b and 4c). In other words, below AMOC strengths of 9 Sv, Blake is still influenced by shallow NADW. As the CAS throughflow is nearly zero in CN00 when the CAS is shallower than $\sim$200 m (Figure 4a), the additional ε_{Nd} decrease of $\sim$1.5 ε_{Nd} units can be attributed to the

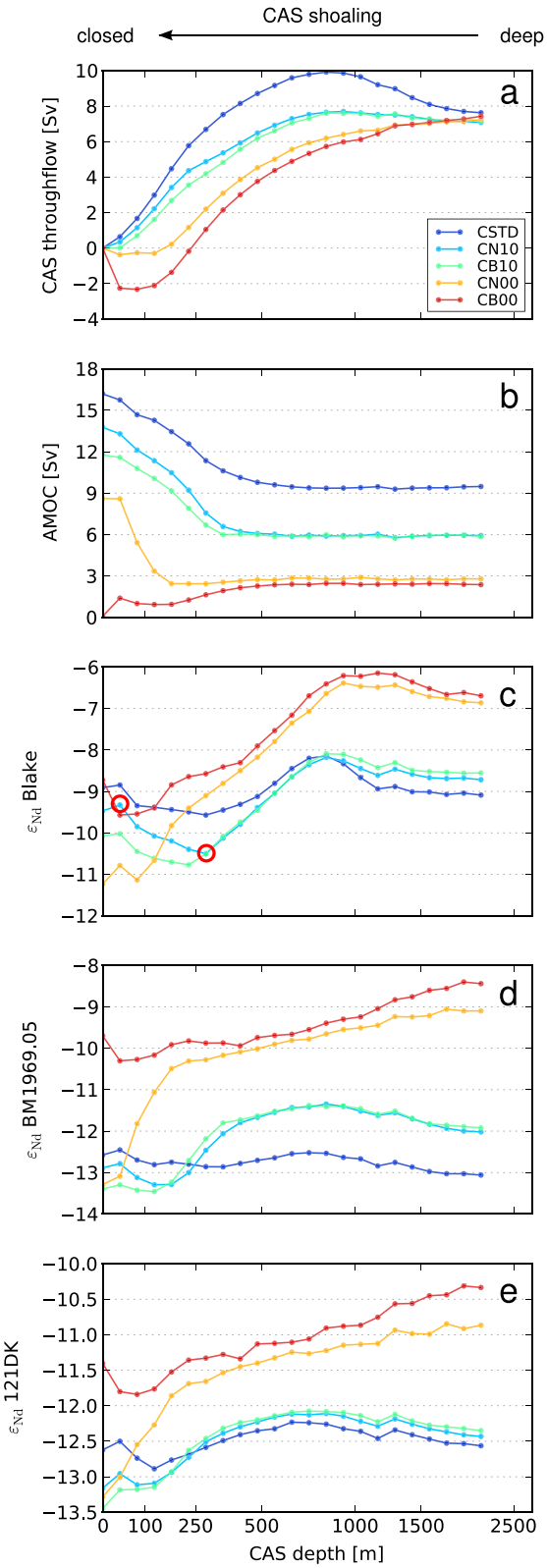

Figure 4. Evolution of (a) the CAS throughflow, (b) AMOC strength, and ε_{Nd} averaged around (c) Blake, (d) BM1969.05, and (e) 121DK, in the CAS shoaling and closure experiments (qualitatively corresponding to a temporal evolution from right to left). Each dot corresponds to the equilibrium value of a separate model simulation. Colors signify different AMOC forcings, where CSTD and CB00 are the experiments with the strongest and weakest AMOC, respectively (Table 1). Red circles in Figure 4c mark two experiments that are further examined in Figure 5.

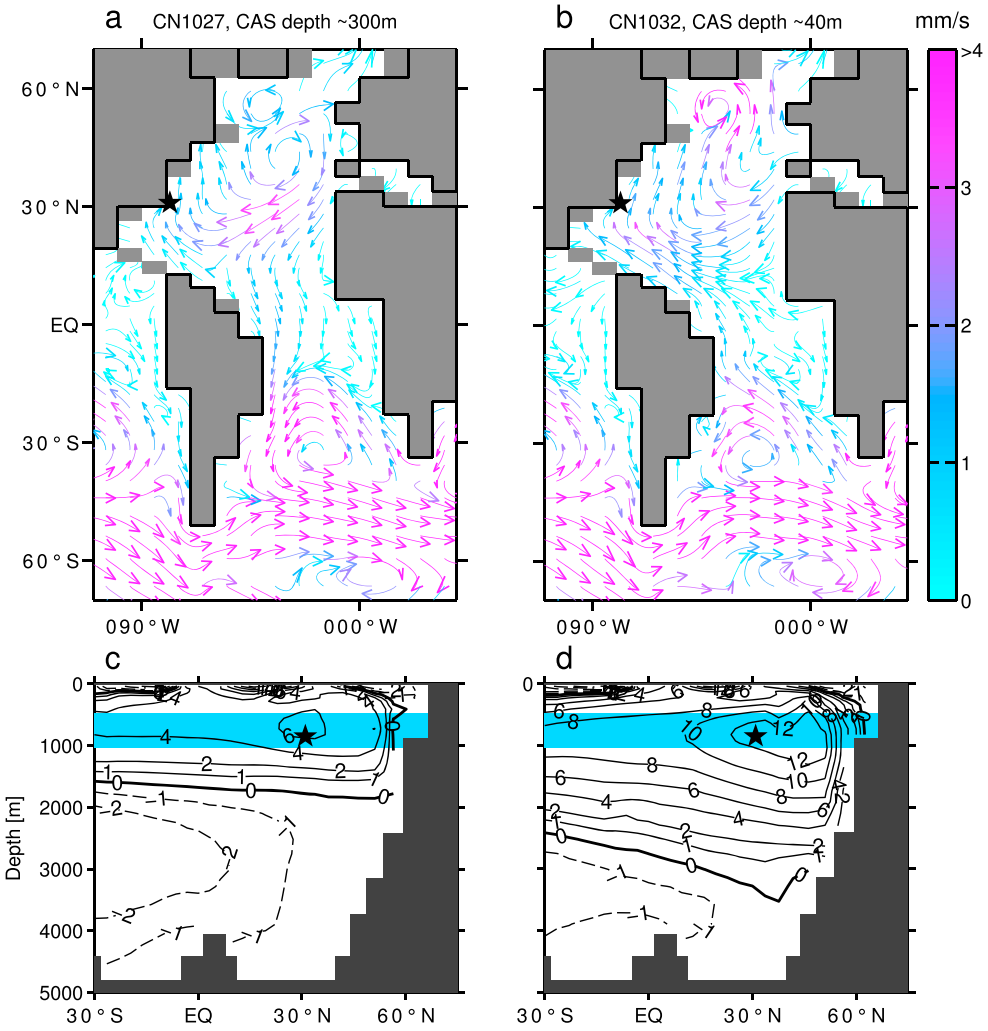

Figure 5. (a, b) Intermediate horizontal circulation, averaged over roughly 500–1000 m depth, in two different experiments with different CAS depths. Flow speed in mm/s along streamlines is shown in colors. Lengths of the arrows are not related to flow speed. (c, d) AMOC in the same experiments. Circulation strength is shown in Sverdrup (10^6 m^3/s), flow is clockwise around positive values. The blue band marks the averaging region of the horizontal circulation shown in Figures 5a and 5b. The Blake location is marked by a star in all panels.

AMOC switch-on from ~3 Sv to ~9 Sv (Figure 4b). This effect is even stronger at the deeper sites (Figures 4d and 4e), as discussed below. No additional decrease occurs in the unrealistic case of a complete AMOC shutdown instead of a switch-on (CB00).

The ε_{Nd} evolution at Site BM1969.05 (Figure 4d) is dominated by the changing influence of NADW, because it is located at a depth of 1850 m where the NADW flow is strong (e.g., Figure 5d). In CSTD, the AMOC amounts to ~ 9 Sv even with a deep CAS (Figure 4b). Therefore, there are only very slight ε_{Nd} changes around BM1969.05, as the site is bathed by NADW at all times. The ε_{Nd} signature remains slightly higher than the ε_{Nd} of NADW (–13.5), probably due to radiogenic boundary source influences. In CN10 and CB10, preshoaling ε_{Nd} values are higher and an ε_{Nd} decrease of ~ 1.5 ε_{Nd} units is simulated in line with the AMOC increase. Only in CN00 and CB00, NADW is weak enough that changes in the eastward CAS throughflow also have a notable impact on ε_{Nd} at Site BM1969.05, namely, a long-term decrease of ~1.5 ε_{Nd} units. However, the effect of the subsequent AMOC switch-on in CN00 is much larger, resulting in an ε_{Nd} decrease of ~3 ε_{Nd} units, while the CAS depth changes by only 200 m.

Site 121DK (Figure 4c) shows a qualitatively very similar ε_{Nd} signal to BM1969.05, although the ranges are smaller. This difference as well as the slightly more variable ε_{Nd} signal in CSTD shows that the NADW influence is not as direct as at BM1969.05. There are three reasons for the similarity: First, the two sites are at

Table 3. Comparison of Modeled and Measured ε_{Nd} Ranges Related to the CAS Shoaling in Three Different Locations (Compare Figure 1)[a]

Location		Model, Med. AMOC	Model, Low AMOC	Geochemical Data
BM1969.05	ε_{Nd}	**–11.3 to –13.5** ***(–2.2)***	**–9.0 to –13.3** ***(–4.3)***	**–10.9 to –13.5** ***(–2.6)***[b]
	CAS depth/time	700 m to 250 m	1900 m to 0 m	3 Ma to the present
	Notable features		$\Delta\varepsilon_{Nd}$ *–3.0* (200 m to 0 m)	
121DK	ε_{Nd}	**–12.1 to –13.4** ***(–1.3)***	**–10.8 to –13.3** ***(–2.5)***	**–10.7 to –11.8** ***(–1.1)***[c]
	CAS depth/time	700 m to 0 m	1900 m to 0 m	3 Ma to the present
	Notable features		$\Delta\varepsilon_{Nd}$ *–1.5* (200 m to 0 m)	
Blake	ε_{Nd}	**–8.1 to –10.8** ***(–2.7)***	**–6.4 to –11.2** ***(–4.8)***	**–7.5 to –11.0** ***(–3.5)***[d]
	CAS depth/time	700 m to 250 m	900 m to 0 m	9 Ma to the present
	Notable features	$\Delta\varepsilon_{Nd}$ *+1.0* (250 m to 0 m)		$\Delta\varepsilon_{Nd}$ *–2.5* (9 Ma to 5 Ma)

[a]For the model, two ranges are given, for medium AMOC (CN10/CB10, compare Table 1) and for low AMOC (CN00). The data ranges correspond to the minimum-to-maximum values of the time intervals presented in the referenced studies. For easier comparison disregarding the offsets, the relative ranges are shown in italics. Additionally, the CAS depth (/time) intervals over which these ε_{Nd} ranges are recorded in the model (/data) are listed. Finally, notable features in the ε_{Nd} evolutions are highlighted (e.g., depth intervals showing a particularly strong ε_{Nd} decrease).
[b]*Burton et al.* [1999].
[c]*Abouchami et al.* [1999].
[d]*Reynolds et al.* [1999].

roughly the same depth; second, the gyre circulation in the North Atlantic allows a zonal exchange of water masses, and third, NADW flow in the North Atlantic is not entirely confined to the western boundary in our model.

On a side note, a slight ε_{Nd} increase (< 1 ε_{Nd} unit) is simulated around all three sites in CB10, CN10, and CSTD for the early CAS shoaling between ~2100 m and ~700 m. This is probably because the flow of NADW through the deep CAS (Figure 3) decreases, such that radiogenic Nd from the Caribbean boundary source remains in the Atlantic instead of being advected into the Pacific. This hypothesis is strengthened by the fact that no increase is recorded for low AMOC forcings (CB00, CN00) around Sites BM1969.05 and 121DK and by results discussed in section 6. However, the increase is not strongest for CSTD around Sites BM1969.05 and 121DK; this may either indicate that the effect is limited by the direct NADW influence in these regions or that other effects contribute to the increase. For CB00 and CN00, an early increase is only found around Blake, suggesting that this is caused by a different, very local effect.

4.3. Model-Data Comparison and Discussion

Because we cannot link the modeled CAS depths to a specific time in the past, we only compare ε_{Nd} ranges of the model simulations to the ranges measured in Fe-Mn crusts (Table 3). Table 3 also indicates the depth or time intervals corresponding to these ε_{Nd} ranges and lists notable changes over partial intervals, which are described in more detail in section 4.2. Results for CB00 and CSTD are not included in the table; CB00 is unrealistic as its modern AMOC is shut down, and CSTD produces much smaller ranges than CN10/CB10. Some processes that could contribute to ε_{Nd} changes [e.g., *Frank et al.*, 1999] are not resolved in our model: i.e., there is no shift in the NADW formation region (not shown) and boundary source changes due to glacial weathering are not simulated. These are referred to as "other processes" in the following.

The simulated ε_{Nd} range around Blake is very similar to the data from *Reynolds et al.* [1999] in case of an intermediate, shallow AMOC (~6 Sv before the shoaling). These model results confirm that the earlier ε_{Nd} decrease *Reynolds et al.* [1999] measured (~2.5 ε_{Nd} units between 9 and 5 Ma, Figure 1b) may have been caused entirely by CAS throughflow changes, if the CAS had shoaled by about 450 m during that time; or alternatively, if a slighter shoaling had caused a throughflow decrease of about 6 Sv (Figure 4a). However, the simulated modern ε_{Nd} value around Blake (~-9.5) is too radiogenic because of an increase during the closure (section 4.2), such that the more recent measured decrease has to be explained by other effects. In case of a sluggish (~3 Sv) preclosure AMOC and an AMOC switch-on in the latest stages of the shoaling, the model produces an even larger ε_{Nd} range than the data. However, the modern ε_{Nd} value only matches the data because the modern model AMOC is too shallow (~9 Sv) in this scenario.

Depending on the AMOC forcing, our model results around BM1969.05 can support either of two common explanations for the latest ε_{Nd} decrease recorded in the data. With a medium AMOC forcing, the simulated ε_{Nd} range is in good agreement with the data, meaning that the measured ε_{Nd} range can almost entirely be explained with changes in unradiogenic NADW inflow. While all NADW is unradiogenic in our model (∼−13.5), this could equivalently be realized by a strengthening of the unradiogenic Labrador seawater contribution to NADW [*Burton et al.*, 1997, 1999; *O'Nions et al.*, 1998]. However, this ε_{Nd} range requires a CAS shoaling of at least 500 m in the model, which most probably did not occur in the last 3 Ma. Therefore, the low AMOC scenario (CN00) is in even better agreement with the hypothesis of *Burton et al.* [1997] and others, as the AMOC switch-on during the CAS closure (from just ∼150 m depth) can explain the full ε_{Nd} range. A sluggish preclosure AMOC is supported by earlier model studies [e.g., *Butzin et al.*, 2011; *Sepulchre et al.*, 2014]. On the other hand, in case of a strong pre-closure AMOC (> 9 Sv) [*Frank et al.*, 2002; *Poore et al.*, 2006], the simulated ε_{Nd} changes around BM1969.05 are very small (Figure 4d, CSTD). Thus, in this scenario the measured ε_{Nd} decrease would have to be explained by other effects, e.g., Northern Hemispheric glaciation [*Frank et al.*, 1999; *von Blanckenburg and Nägler*, 2001; *Muiños et al.*, 2008].

Around the East Atlantic Site 121DK, the model ε_{Nd} range is also most similar to the data for an intermediate AMOC. However, the agreement of the absolute values is worse than in the West Atlantic, with a shift toward too unradiogenic values. This is also the case for other deep sites in the East Atlantic that can be compared to data from *Muiños et al.* [2008] (not shown). While this offset may partly be explained by the boundary source uncertainty, it mainly reflects the model's overestimation of NADW influence in the West Atlantic. On another note, *Muiños et al.* [2008] have measured larger ε_{Nd} ranges than the model simulates in the East Atlantic (∼ 2.5 ε_{Nd} units). Although the model can reproduce this range in the low AMOC scenario, the corresponding CAS depth range is unrealistic for the last 10 Ma (∼ 2000 m), suggesting that their records may also be influenced by processes not resolved in the model.

In summary, the model results favor a relatively slow and shallow (∼ 6 Sv) AMOC before the CAS shoaling to depths smaller than ∼ 700 m, if the circulation changes in response to the shoaling should explain large parts of the measured ε_{Nd} changes in the North Atlantic. This is strengthened by the absolute ε_{Nd} values at the two West Atlantic sites, which are in good agreement with the earliest data (deviation −0.4 to −0.6 ε_{Nd} units). A nearly shut down (∼ 3 Sv) preclosure AMOC produces too large ranges and too radiogenic ε_{Nd} values in the West Atlantic (+1.1 to +1.9 ε_{Nd} units) and is therefore less plausible based on our model, but still possible considering the uncertainties (sections 6 and 7). With a stronger preclosure AMOC (>9 Sv), the contribution of the modeled circulation effects is small (∼1.4 ε_{Nd} units around Blake and ∼0.5 ε_{Nd} units around BM1969.05).

5. Opening and Deepening of the Drake Passage

5.1. Circulation Changes

An opening of DP in the Bern3D modified modern bathymetry (EOCTRL) results in an eastward throughflow at all depth levels. This is in agreement with other models using both modern and paleobathymetries with an open DP [e.g., *Lefebvre et al.*, 2012]. Due to the strong wind stress forcing, flow is strongest at the surface and decreases with depth.

Figure 6 displays the DP and CAS throughflows, AMOC and SOMOC strength, and seafloor ε_{Nd} responses in the five DP deepening experiments with different AMOC forcings (section 2.3). The DP throughflow (Figure 6a, solid lines) is nearly independent of the AMOC forcing. It already amounts to roughly 9 Sv for the shallowest (∼40 m) DP opening and increases to a maximum of about 60 Sv when the passage is deepened. The steplike throughflow increase at a depth of roughly ∼ 1300 m is due to a reduction of the model's boundary drag in cells with a seafloor depth greater than this threshold value, and can thus be considered a model artifact. The slower increase before this step, and the slight decrease thereafter, suggest that the throughflow approaches an equilibrium somewhat below 60 Sv. The magnitude of this maximum is probably constrained by the bathymetry, grid resolution, wind stress forcing, and drag.

The net eastward CAS throughflow (Figure 6a, dashed line) is closely linked to the DP throughflow, because it develops from a branch of the ACC (section 3). It weakens as DP is opened and deepened, because a larger portion of the wind forcing is transferred to the strengthening ACC (see also Figures 2e and 2f). The influence of the AMOC forcing on the throughflow only becomes important when DP is opened to depths larger

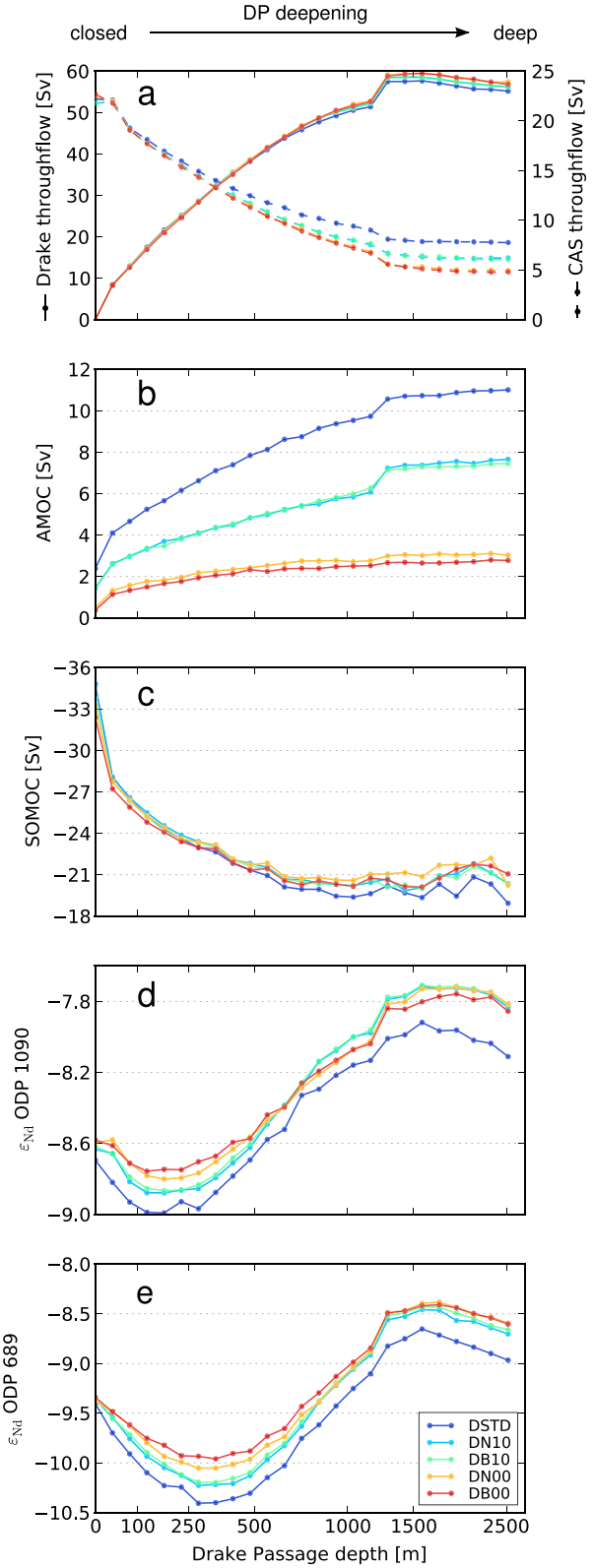

Figure 6. Evolution of (a) the DP (solid line) and CAS (dashed) throughflows, (b) AMOC strength, (c) SOMOC strength), and ε_{Nd} averaged around ODP Sites (d) 1090 and (e) 689, in the DP opening and deepening experiments (qualitatively corresponding to a temporal evolution from left to right). Each dot corresponds to the equilibrium value of a separate model simulation. Colors signify different AMOC forcings, where DSTD and DB00 are the experiments with the strongest and weakest AMOC, respectively (Table 1).

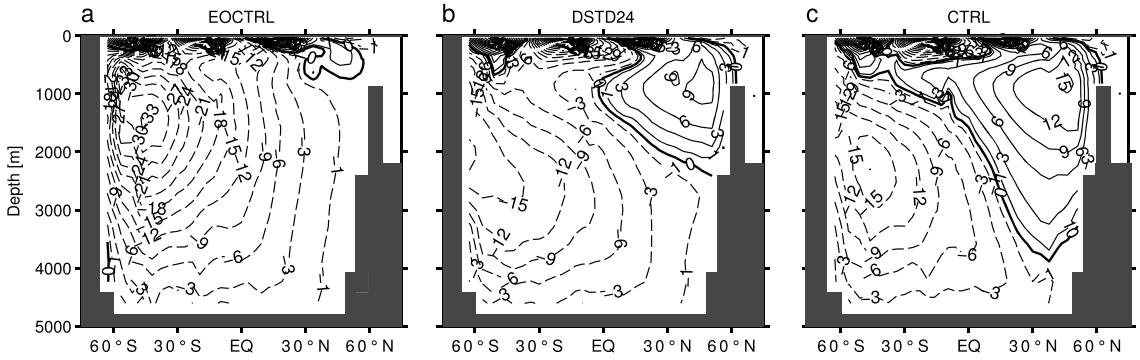

Figure 7. Global Meridional Overturning Circulation (GMOC) in three different bathymetries: (a) ~1300 m open CAS with closed Drake Passage (EOCTRL); (b) open CAS with ~ 2500 m deep Drake Passage (DSTD24); and (c) modern (CTRL). Circulation strength is shown in Sverdrup (10^6 m^3/s), and flow is clockwise around positive values.

than ~ 500 m. In these cases, a stronger forcing (i.e., larger interbasin salinity gradient) enhances the CAS throughflow, like in the CAS-only experiments (Figure 4a).

For all DP depths, AMOC strengths in DN10 and DB10 (or DN00 and DB00) are very similar (Figure 6b). Thus, like in the CAS experiments (Figure 4b), the southern component of the AMOC forcing has a much smaller impact than the northern component. The "Drake Passage effect" (section 1 or *Toggweiler and Samuels* [1995]) is also visible in Figure 6b: The AMOC increases from very sluggish to up to 11 Sv (despite the open CAS) as DP is opened and deepened. Because this effect is enhanced by the AMOC forcing, it is most pronounced in DSTD.

Figure 6c shows the SOMOC response to the DP opening and deepening. Widely consistent with previous modeling studies [*Mikolajewicz et al.*, 1993; *Sijp and England*, 2004; *Sijp et al.*, 2009, 2011; *Cristini et al.*, 2012], the opening substantially weakens the SOMOC. The magnitude of the weakening in our model is best comparable to what *Sijp et al.* [2011] found with an open versus closed DP in an Eocene bathymetry. The weakening of the SOMOC and strengthening of the AMOC from EOCTRL to DSTD24 is readily visible in the Global Meridional Overturning Circulation (GMOC, Figures 7a and b7). The CTRL GMOC with a more vigorous AMOC is also shown for comparison (Figure 7c).

5.2. The ε_{Nd} Response in the Atlantic Sector of the Southern Ocean

Here we discuss the ε_{Nd} response in the DP experiments around ODP Sites 1090 (Figure 6d) and 689 (Figure 6e). Both sites show an overall ε_{Nd} increase as DP deepens, which is however preceded by a decrease in response to the DP opening. The increase is linked to the strengthening ACC which transports radiogenic Pacific waters into the Atlantic sector of the Southern Ocean. The shallower (1600 m) Site ODP 689 is directly affected by the horizontal DP throughflow if DP is deep enough; furthermore, this site is influenced by the downward propagation of AABW, which also gets more radiogenic as DP deepens. This may explain why the increase is stronger around ODP 689 (~ 1.5–1.8 ε_{Nd} units) than around the deeper Site ODP 1090 (~ 1.1–1.2 ε_{Nd} units), which is only indirectly reached by the radiogenic DP throughflow (i.e., via AABW or Circumpolar Deep Water (CDW)).

The initial ε_{Nd} decrease is also much more pronounced around ODP 689 (~ 0.6–1.0 ε_{Nd} units) than around ODP 1090 (~0.2–0.3 ε_{Nd} units). This hints to four possible mechanisms that could cause the decrease in the model: (i) an increased inflow of relatively unradiogenic NADW due to the strengthening AMOC (AMOC effect), (ii) local shifts in circulation patterns toward less radiogenic source waters (source effect), (iii) a decreased inflow of North Pacific waters due to weakening CAS throughflow (CAS effect), and (iv) a decreased inflow of relatively radiogenic Antarctic Bottom Water (AABW) due to the reduced SOMOC (SOMOC effect) [*Rempfer et al.*, 2012a].

The source effect is apparently negligible, as a very similar ε_{Nd} decrease is still simulated when the boundary source is modified (section 6). The AMOC effect can account for a decrease of ~0.4 ε_{Nd} units at ODP 689, which is the difference between the decrease ranges in the strongest and the weakest (near zero) AMOC scenarios. This leaves the combined CAS and SOMOC effects as the prime causes of the decrease. Note that the

Table 4. Comparison of Modeled and Measured ε_{Nd} Ranges Related to the DP Deepening in Two Different Locations (Compare Figure 1)[a]

Location		Model, Medium AMOC	Geochemical Data
ODP 1090	ε_{Nd}	**–8.9 to –7.7** ***(+1.2)***	**–8.5 to –5.2** ***(+3.3)***[b]
	DP depth/time	200 m to 1600 m	42 Ma to 34 Ma
	Notable features	$\Delta\varepsilon_{Nd}$ *–0.3* (0 m to 150 m)	$\Delta\varepsilon_{Nd}$ *+2.9* (42 Ma to 39 Ma)
ODP 689	ε_{Nd}	**–10.2 to –8.4** ***(+1.8)***	**–9.4 to –7.3** ***(+2.1)***[b]
	DP depth/time	350 m to 1600 m	42 Ma to 35 Ma
	Notable features	$\Delta\varepsilon_{Nd}$ *–0.9* (0 m to 300 m)	

[a]Model ranges with an intermediate AMOC forcing (CN10/CB10) are shown. The data ranges correspond to the minimum-to-maximum values of the time intervals presented in the referenced studies. For easier comparison disregarding the offsets, the relative ranges are shown in italics. Additionally, the DP depth (/time) intervals over which these ε_{Nd} ranges are recorded in the model (/data) are listed. Finally, notable features in the ε_{Nd} evolutions are highlighted (e.g., depth intervals showing an ε_{Nd} decrease).
[b]*Scher and Martin* [2006].

mechanisms causing the decrease have to be more substantial than meets the eye, as they must counteract the rapid onset of the ACC, which is expected to increase ε_{Nd} in the region.

In the modern bathymetry, the SOMOC effect was demonstrated to have a great impact on ε_{Nd} in the Atlantic sector of the Southern Ocean [*Rempfer et al.*, 2012a]. However, the effect is weaker in the bathymetries with a shallow or closed DP, because the difference between the Atlantic and AABW ε_{Nd} signatures is small in these bathymetries. This is shown in Figure 2f for a closed DP, ε_{Nd} distributions with a shallow DP are similar. The SOMOC decrease may still contribute to the ε_{Nd} decrease, especially around ODP Site 689 which is bathed by downward flowing AABW, but it is probably not as influential as the CAS effect.

We therefore suggest that the diminishing CAS throughflow is probably the dominant cause of the simulated ε_{Nd} decrease in response to the DP opening. The vigorous CAS throughflow is advected southward as a western boundary current at intermediate depths (~ 200–1300 m). This flow is so strong that it is readily visible in the barotropic circulation (Figure 2e). Thereby, the CAS throughflow supplies radiogenic Nd to the Southern Ocean. A weakening of this intermediate inflow decreases ε_{Nd} at ODP Site 689, but also at ODP Site 1090, as the inflow eventually feeds into CDW and/or AABW. Because the CAS throughflow is probably too strong in our model (section 7), one might argue that the ε_{Nd} decrease may be overestimated as well. On the other hand, a weaker CAS throughflow would enable an enhanced AMOC, resulting in an increased southward flow of unradiogenic NADW at intermediate depths, which may cause a similar ε_{Nd} decrease.

A second, less pronounced ε_{Nd} decrease is simulated for the deepest DP depths (Figures 6d and 6e). It is probably related to both the slight DP throughflow weakening and AMOC strengthening (Figures 6a and 6b). This is further examined with additional experiments that are discussed in section 5.4.

5.3. Model-Data Comparison and Discussion

The ε_{Nd} response in the DP simulations is less strongly influenced by the AMOC forcings than in the CAS simulations, because the NADW influence in the Southern Ocean is limited due to the vigorous SOMOC. Because the ranges are thus similar for all forcings (Figures 6d and 6e), we only compare the modeled ε_{Nd} range with intermediate AMOC forcing (CN10/CB10) to the sediment core data from *Scher and Martin* [2006] (Table 4).

The measured ε_{Nd} range is larger at ODP Site 1090 (~ 3.3 ε_{Nd} units) than at OPD Site 689 (~ 2.1 ε_{Nd} units). *Scher and Martin* [2006] argue that a DP opening may have transported radiogenic Pacific waters to AABW formation regions, and AABW may have influenced Site 1090 more directly than the shallower Site 689.

The circulation and ε_{Nd} changes in our model differ from this hypothesis. An ε_{Nd} decrease is simulated in the first stages of the DP opening (Figures 6d and 6e), which is not observed in the data from *Scher and Martin* [2006] (Figure 1d). However, the few measurements preceding the increase do not exclude the possibility of such an initial decrease. This means that DP may have opened earlier than the onset of the observed ε_{Nd} increase, corroborating findings of, e.g., *Livermore et al.* [2005] and *Eagles et al.* [2006]. We will, however, not venture to draw this conclusion. While the delayed increase is robust within our sensitivity experiments,

it is subject to considerable uncertainties (section 7). The CAS throughflow changes contributing to this decrease may be specific to our model setup, but the also contributing AMOC increase and SOMOC decrease are in agreement with earlier model studies on the DP opening [*Mikolajewicz et al.*, 1993; *Sijp and England*, 2004; *Sijp et al.*, 2009, 2011; *Cristini et al.*, 2012]. Our model experiments cannot answer the question whether the AMOC and SOMOC changes alone could induce an ε_{Nd} decrease strong enough to counteract the increase due to a more radiogenic AABW signature.

While AABW formation in the model mainly takes place close to Antarctica, the model resolution is too coarse to confine the downward propagation of AABW so tightly that ODP Site 689 is not bathed by AABW (e.g., Figures 1a and 7a). Therefore, ODP Site 689 is probably more strongly influenced by AABW than Site 1090 in our model, which explains the larger ε_{Nd} increase range for DP depths >300 m. On another note, the modern AABW influence in the deep Atlantic is underestimated in the Bern3D model [*Gerber and Joos*, 2013]; while it is much larger in the bathymetries with a shallow DP, it may still be underestimated. However, even with a stronger AABW influence, the simulated ε_{Nd} range at Site 1090 could probably not be much larger than at Site 689, i.e., still smaller than the observed range. This discrepancy could only be reconciled if the initial ε_{Nd} decrease was replaced by a steep increase, for which we do not find a plausible mechanism in our model. Therefore, we argue based on the model results, that effects other than the inflow of radiogenic Pacific waters may have contributed to the measured strong ε_{Nd} increase at Site 1090, e.g., local circulation changes or changes in the boundary source. *Scher and Martin* [2006, 2008] present paleoceanographic evidence against most plausible mechanisms other than the inflow of Pacific Waters; therefore, further model simulations with more highly resolved models are required to unravel the role of the DP opening and other effects in the ε_{Nd} evolution of Site 1090.

Opposed to Site 1090, the ε_{Nd} range at Site 689 is in reasonable agreement with the data. While a DP deepening to a depth of ~1300 m is required to achieve this ε_{Nd} range, this depth corresponds to a DP throughflow of only 60 Sv in the model (due to the underestimation of the ACC). This throughflow strength, and thereby also the induced ε_{Nd} range, may correspond to a shallower DP depth in reality, considering that the modern DP throughflow amounts to 134 Sv [*Cunningham et al.*, 2003].

5.4. Freshwater Experiments Following the DP Deepening

Following the ε_{Nd} increase related to the DP opening, *Scher and Martin* [2008] also found an ε_{Nd} decrease in the ODP 1090 sediment core (Figure 1d, white background). This decrease is much stronger than the one simulated by our model (Figure 6d, DP depth > 1500 m), amounting to roughly 3 ε_{Nd} units (minimum to maximum, neglecting some interruptions of the decrease). *Scher and Martin* [2008] suggest an enhanced NADW export to the Southern Ocean in response to the DP deepening as a cause for this ε_{Nd} decrease. Therefore, freshwater experiments were conceived (section 2.4) to test whether a stronger AMOC increase following the DP deepening could cause a comparable ε_{Nd} decrease in the model.

Although the freshwater perturbations are limited to the North Atlantic, they also strongly influence the CAS throughflow and, thereby, the DP throughflow and SOMOC. Therefore, we do not consider this a realistic framework for a model-data comparison. While an ε_{Nd} decrease is simulated around ODP Site 1090, it is much weaker than the observed decrease [*Scher and Martin*, 2008], which is at least partly due to the counteracting influences of other circulation changes provoked by the artificial freshwater forcing.

A scatterplot matrix indicates the interactions between multiple variables (Figure 8). In our case, the variables are the four most important circulation features (CAS and DP throughflows, AMOC, and SOMOC) and ε_{Nd} at ODP Sites 1090 and 689, as well as the prescribed freshwater forcing (which is the only independent variable).

Note that not all of the apparent correlations signify a direct dependence between the correlated variables. This is reflected in the background coloring of the panels, which is based on the authors' interpretation of the model results. The panels with a light grey background mark variable pairs that are only indirectly related (i.e., via another circulation feature). For example, the freshwater forcing only has a direct influence on the CAS throughflow and AMOC (Figures 8a and 8c), which in turn influence the other variables. Panels are given a dark grey background if the sign of the correlation is different from the physical expectation (e.g., Figure 8e, described further below). This means that the two shown variables are less strongly influenced by one another than by a different variable, which results in the depicted indirect correlation overruling their expected correlation. In Figures 8l–8n, the correlation is reversed for very small freshwater forcings.

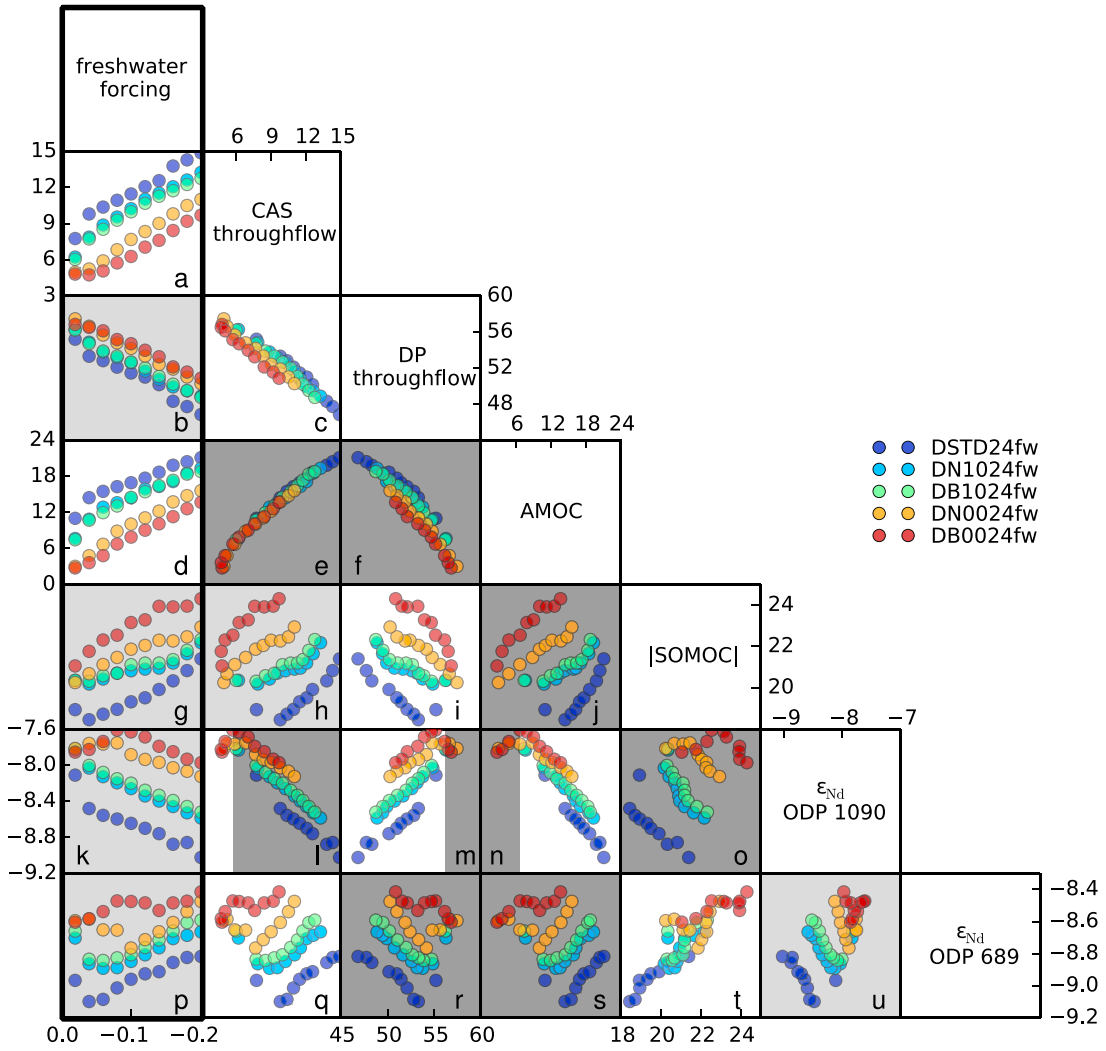

Figure 8. Freshwater experiments following the Drake Passage (DP) deepening experiments, i.e., in the bathymetry with the deepest (~2500 m) DP. Negative freshwater fluxes of −0.02 to −0.20 Sverdrup (10^6 m^3/s) are prescribed the North Atlantic (section 2.4). Six dependent variables (CAS and DP throughflow, AMOC, SOMOC, and ε_{Nd} averaged around ODP Sites 689 and 1090) are plotted against the independent variable (the prescribed freshwater forcing) and against each other. Units are Sverdrup for the top five variables, and ε_{Nd} units for the bottom two. Light grey and dark grey backgrounds mark panels where the correlation is mainly indirect (i.e., via one or more other variables), dark grey regions show correlations whose sign is opposite to the physical expectations (compare text). Colors signify different AMOC forcings, where DSTD24fw and DB0024fw are the experiments with the strongest and weakest AMOC, respectively (Table 1).

These panels therefore have a split background, where dark grey starts at the data point from which on the correlation is opposite to expectations (for all AMOC forcings).

The following observations apply for each AMOC forcing (color) separately; we do not make statements across different forcings, as we consider them to be separate scenarios. The DP throughflow decreases in response to the forced CAS throughflow increase (Figure 8c). The strong anticorrelation between the two throughflows was also found in the DP deepening experiments (Figure 6a). The AMOC is most directly controlled by the freshwater forcing, which causes it to increase (Figure 8d) despite the increasing CAS throughflow (Figure 8e) and decreasing DP throughflow (Figure 8f). The SOMOC strength increases (Figure 8g), indicating that its negative correlation with the DP throughflow (Figure 8i) is stronger than its normally negative correlation with the AMOC, which is overruled (Figure 8j). While the CAS throughflow may also have a direct impact on the SOMOC (Figure 8h), the indirect impact via DP throughflow (Figure 8i) is probably more important, which is why a light grey background was chosen for (Figure 8h).

In contrast to the DP deepening experiments, the ε_{Nd} changes in response to the freshwater forcing are mostly opposite at ODP Sites 689 and 1090 (Figures 8k, 8p, and 8u), except for the weakest freshwater

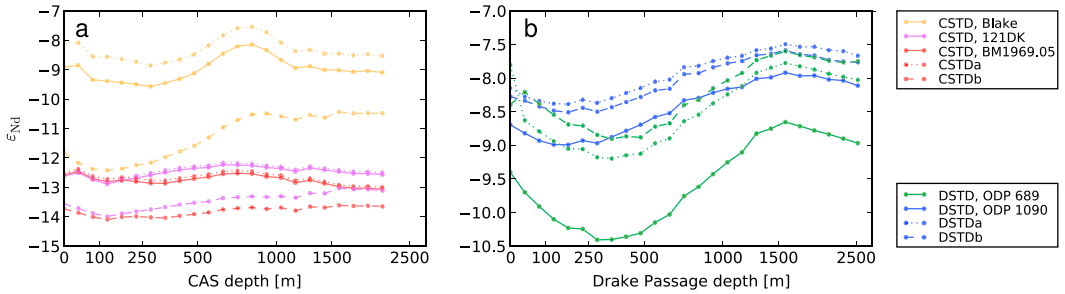

Figure 9. Boundary source sensitivity study for (a) the CAS experiments and (b) the Drake Passage experiments. Spatially averaged ε_{Nd} evolutions around (a) Sites BM1969.05, 121DK, and Blake, and (b) ODP Sites 689 and 1090 are plotted. Colors correspond to Figure 1. The experiments with unmodified boundaries (CSTD/DSTD) are shown as solid lines, the ones with a modified boundary source in the Caribbean/Antarctic (CSTDa/DSTDa) as dotted lines, and the ones with no boundary source in these regions (CSTDb/DSTDb) as dashed lines (section 2.5).

forcings. This allows us to infer which circulation effects dominate the ε_{Nd} signal at each site. For ε_{Nd} in the Southern Ocean, we expect a positive correlation with CAS throughflow, DP throughflow and SOMOC strength, and a negative correlation with AMOC strength. Since the correlations are mostly of opposite sign in Figures 8l, 8o, 8r, and 8s, we deduce that these influences are weaker. We infer that ODP Site 689 is most strongly influenced by the combined effects of CAS and SOMOC changes (Figures 8q and 8t). This is because the site is relatively shallow and bathed by downward propagating AABW. However, the influences of DP throughflow and AMOC are apparently only slightly weaker, as the ε_{Nd} changes are very small at this site, and particularly nonlinear for low freshwater and/or AMOC forcings. ODP Site 1090 on the other hand, is mainly influenced by the combined effects of DP throughflow and AMOC changes (Figures 8m and 8n). As this site lies deeper than the main DP throughflow and NADW in our model, these signals are probably transported to the site by CDW. Note, however, that these findings are not necessarily applicable for, e.g., bathymetries with a shallow DP, in which the ε_{Nd} distribution prior to circulation changes is different.

6. Boundary Source Modifications

Boundary source modifications that were applied in experiments CSTDa, CSTDb, DSTDa, and DSTDb (Table 1) do not considerably alter the qualitative trends in the ε_{Nd} evolutions (Figure 9). This confirms that the signals we have discussed above are indeed primarily caused by ocean circulation changes. However, the boundary source modifications shift the absolute ε_{Nd} values. These shifts are largest for the shallowest sites (Blake and ODP 689). Note that modifications are quite drastic in CSTDb and DSTDb; therefore, the actual boundary source uncertainty is probably smaller than these shifts indicate. The unmodified experiments (CSTD/DSTD) should still produce the most realistic values, as the magnitude of the boundary source was tuned (along with other parameters) to best reproduce the present-day ε_{Nd} as well as dissolved Nd concentrations [*Rempfer et al.*, 2011].

In the CAS experiments (Figure 9a), two slight trend deviations are caused by boundary source modifications in addition to the shifts. First, the slight ε_{Nd} increase in CSTD for the deep shoaling ($\sim$ 2100–700 m) vanishes around all sites when the Caribbean boundary source is removed (CSTDb). This confirms that this increase in CSTD (and CN10, CB10) may be caused by the weakening advection of radiogenic Caribbean waters out of the Atlantic as the CAS shoals (section 4.2). Second, the ε_{Nd} increase at Blake in the final stages of the shoaling is less pronounced in CSTDb than in CSTD. This is because the AMOC return flow, which is mixed with Caribbean waters before reaching Blake (Figure 5b), is less radiogenic in CSTDb. If the Caribbean boundary source was not removed, but less radiogenic (as suggested by *Osborne et al.* [2014]), changes in ε_{Nd} evolutions would probably be similar, but less pronounced.

In the DP experiments, trend deviations are only notable around ODP Site 689 for the very first opening step, probably because this step causes a strong SOMOC change which is sensitive to the Antarctic boundary source. Except for this first step, the ε_{Nd} shift is very similar in DSTDa and DSTDb, suggesting that the influence of the Antarctic boundary source toward more negative values is mainly caused by the single most negative boundary source cell.

In summary, uncertainties associated with the boundary source call for caution, especially in the interpretation of simulated changes in ε_{Nd} for very shallow openings. However, these uncertainties may also partly explain simple offsets between measured and simulated ε_{Nd} evolutions. For intermediate CAS and DP openings, the fact that boundary source modifications do not alter the qualitative ε_{Nd} evolution strengthens the confidence in the interpretations of simulated ε_{Nd} changes.

7. Limitations

The main limitations of this sensitivity study fall into two categories: boundary conditions and model limitations. These are obviously linked: e.g., the coarse model resolution constrains the amount of detail in the tectonic boundary conditions (i.e., the bathymetry). Apart from that, the largest deviation from realistic boundary conditions is induced by our choice of present day boundary conditions for both bathymetry and climate. This probably has a larger impact on the DP experiments [e.g., *Heinemann*, 2009; *Zhang et al.*, 2010], but could also significantly influence the CAS experiments, as the shoaling may have taken place predominantly before 10 Ma [*Montes et al.*, 2012a]. However, choosing present day boundary conditions has the advantage of enabling a sensitivity study purely on the effects of the two seaways (CAS and DP), without tackling the large uncertainties related to tectonic boundary conditions [e.g., *Barker et al.*, 2007; *Molnar*, 2008].

Model limitations include the frictional geostrophic formulation, inducing the underestimation of some circulation features in the present day bathymetry (i.e., the ACC and AABW in the Atlantic sector of the Southern Ocean). Also, while the EBM can account for temperature changes as well as evaporation and precipitation adjustments, it cannot produce a dynamical atmospheric response, and the wind stress remains prescribed to present-day level. This is reasonable, as *von der Heydt and Dijkstra* [2006] have found in a GCM that wind stress over the ocean with Miocene and Oligocene conditions differs only slightly from present day.

Furthermore, there are uncertainties related to our approach for the simulation of Nd. As the boundary source has the strongest impact on the ε_{Nd} distribution [*Rempfer et al.*, 2012b], the most critical simplification for a paleoceanographic study remains that this source is set to modern values, which have been interpolated from *Jeandel et al.* [2007]. However, *Rempfer et al.* [2012b] have shown that very large source modifications would be necessary to achieve ocean-wide ε_{Nd} changes of magnitudes comparable to the changes found in geochemical data. This means that, while the uncertainty of the model results is increased due to this simplification, qualitative or semiquantitative statements on the past evolution of ε_{Nd} based on the model are possible.

The direction and magnitude of the CAS throughflow is a source of great uncertainty for the ε_{Nd} response to a DP opening and deepening. Other models with a shallow or closed DP (mostly in a paleobathymetry) show a net throughflow that is either eastward [e.g., *Heinemann*, 2009, Figure 4.2] or westward [e.g., *Sijp et al.*, 2011, Figure 5] but weaker than in our simulations in both cases. Thus, the eastward transport through CAS is probably overestimated in our model. The main reasons for this are probably the lack of flow constriction in the CAS region due to the coarse resolution, as well as the lack of an open Tethys Seaway [e.g., *von der Heydt and Dijkstra*, 2006].

8. Summary and Conclusions

1. The attribution of the ε_{Nd} changes in the North Atlantic during the last 10 Ma to circulation changes and other effects is highly dependent on the preclosure AMOC strength. By preclosure, we refer to a CAS depth of roughly 400 m, because the AMOC strength starts to change only when the CAS shoals to shallower depths than this threshold.
2. For a sluggish ($\sim$ 3 Sv) preclosure AMOC, an AMOC switch-on in response to the CAS closure causes ε_{Nd} decreases of $\sim 3.0\,\varepsilon_{Nd}$ units at Site BM1969.05, $\sim 1.5\,\varepsilon_{Nd}$ units at Site 121DK, and $\sim 1.2\,\varepsilon_{Nd}$ units at Blake. In this scenario, even if some of these ranges are overestimated, ε_{Nd} decreases during the last 3 Ma could entirely be explained by such an AMOC switch-on (or a switch-on of Labrador Sea Water formation).
3. We consider a shallow ($\sim$6 Sv) preclosure AMOC to be the most probable scenario based on the model-data agreement, as most measured ε_{Nd} changes can be explained by the simulated circulation changes. Only the most recent changes cannot be fully explained, suggesting a contribution of other effects, e.g., Northern Hemispheric glaciation.

4. For an active (>9 Sv) preclosure AMOC, modeled circulation effects alone can explain none of the observed ε_{Nd} changes. Especially at Site BM1969.05, the simulated ε_{Nd} changes are very small, such that the measured decrease must entirely be explained by unresolved effects in this scenario.
5. Assuming the sluggish or shallow AMOC scenario, the measured 2.5 ε_{Nd} decrease at Blake at 9–5 Ma can entirely be explained by CAS throughflow changes, if the CAS was at least 700 m deep at 9 Ma. In the active AMOC scenario, the modeled throughflow changes can only explain about half of that increase.
6. When the AMOC strengthens, it also deepens in our model. This causes an ε_{Nd} increase in the shallow North Atlantic, because the influence of shallow NADW decreases and the influence of the relatively radiogenic AMOC return flow increases. If such an AMOC deepening took place during the CAS shoaling, other effects may have counteracted this possible ε_{Nd} increase, because no such increase is measured at Blake.
7. Our model and other EMICs indicate water mass transport from the Atlantic to the Pacific through the deep CAS, exporting radiogenic Nd from the Caribbean boundary source out of the Atlantic. The deep CAS shoaling prevents this export, thus causing a slight ε_{Nd} increase in the North Atlantic.
8. In the DP deepening and freshwater experiments, a strong anticorrelation between the eastward CAS and DP throughflows is found. Because the CAS throughflow is very strong when DP is closed or shallow, it has a pronounced influence on ε_{Nd} in the Atlantic sector of the Southern Ocean.
9. The decreasing CAS throughflow, along with contributions of the decreasing SOMOC and increasing AMOC, causes an initial ε_{Nd} decrease around ODP Sites 1090 and (more notably) 689 in response to the simulated DP opening. This could mean that DP opened even earlier than the measured ε_{Nd} increase; if these sites were indeed influenced by the CAS throughflow or if SOMOC and AMOC changes alone were strong enough to counteract the ε_{Nd}-increasing effect of Pacific waters. However, the simulated decrease could also be specific to our model setup, due to an overestimated CAS throughflow and other uncertainties.
10. Following this decrease, the DP deepening causes an ε_{Nd} increase that is in reasonable agreement with the data for ODP Site 689, but much weaker for Site 1090. The AABW influence at Site 1090 may be underestimated, and the influence of the decreasing CAS throughflow may further diminish the simulated range. Even without these effects however, our model cannot achieve the measured ε_{Nd} range at Site 1090. This indicates either that the model does not fully capture the circulation response to the DP deepening, or that unresolved effects (i.e., local circulation shifts or boundary source changes) may have contributed to the measured ε_{Nd} increase.
11. In our model, the influence of the AMOC increase in response to the DP deepening is too weak to cause a strong ε_{Nd} decrease at ODP Site 1090.
12. Freshwater perturbation experiments in an open CAS/deep DP bathymetry indicate that ε_{Nd} at ODP Site 689 is most strongly influenced by combined changes in the CAS throughflow and SOMOC, while the dominant influences at Site 1090 are AMOC and DP throughflow changes. Furthermore, the SOMOC strength is more directly influenced by DP throughflow changes than AMOC changes.
13. Boundary source modifications cause ε_{Nd} shifts, but no qualitative changes in ε_{Nd} evolutions except for very shallow CAS/DP (or very deep CAS). This strengthens the confidence in the model results for intermediate seaway depths but calls for cautious interpretation of the ε_{Nd} response to very shallow openings (at shallow sites, i.e., Blake and ODP 689).
14. It is suggested that the DP deepening experiments, especially the opening to shallow depths of up to ~300m, are repeated in a more comprehensive and highly resolved model. An Eocene or Oligocene paleobathymetry should be used to account for the open Tethys Seaway and narrow Tasmanian Gateway in addition to the open CAS and shallow DP. It is crucial to constrain the nature and magnitude of the CAS and Tethys Seaway throughflows during this period, in order to better understand the ε_{Nd} changes in the Atlantic and Southern Oceans.

Acknowledgments
We thank Martin Frank and two anonymous reviewers for their constructive comments that have helped to substantially improve the manuscript. We acknowledge support by the Swiss National Science Foundation through project 200020_147174. The model results presented in this study are available from the corresponding author upon request (pfister@climate.unibe.ch).

References

Abouchami, W., S. Galer, and A. Koschinsky (1999), Pb and Nd isotopes in NE Atlantic Fe-Mn crusts: Proxies for trace metal paleosources and paleocean circulation, *Geochim. Cosmochim. Acta*, *63*(10), 1489–1505, doi:10.1016/S0016-7037(99)00068-X.

Arsouze, T., J.-C. Dutay, F. Lacan, and C. Jeandel (2007), Modeling the neodymium isotopic composition with a global ocean circulation model, *Chem. Geol.*, *239*(1–2), 165–177, doi:10.1016/j.chemgeo.2006.12.006.

Barker, P. F., G. M. Filippelli, F. Florindo, E. E. Martin, and H. D. Scher (2007), Onset and role of the Antarctic circumpolar current, *Deep Sea Res. Part II*, *54*(21–22), 2388–2398, doi:10.1016/j.dsr2.2007.07.028.

Bertram, C., and H. Elderfield (1993), The geochemical balance of the rare earth elements and neodymium isotopes in the oceans, *Geochim. Cosmochim. Acta*, *57*(9), 1957–1986, doi:10.1016/0016-7037(93)90087-D.

Bijl, P. K., et al. (2013), Eocene cooling linked to early flow across the Tasmanian Gateway, *Proc. Natl. Acad. Sci. U.S.A.*, *110*(24), 9645–9650, doi:10.1073/pnas.1220872110.

Burton, K. W., H. F. Ling, and R. K. ONions (1997), Closure of the Central American Isthmus and its effect on deep-water formation in the North Atlantic, *Nature*, *386*(6623), 382–385, doi:10.1038/386382a0.

Burton, K. W., D.-C. Lee, J. N. Christensen, A. N. Halliday, and J. R. Hein (1999), Actual timing of neodymium isotopic variations recorded by FeMn crusts in the western North Atlantic, *Earth Planet. Sci. Lett.*, *171*(1), 149–156, doi:10.1016/S0012-821X(99)00138-7.

Butzin, M., G. Lohmann, and T. Bickert (2011), Miocene ocean circulation inferred from marine carbon cycle modeling combined with benthic isotope records, *Paleoceanography*, *26*, PA1203, doi:10.1029/2009PA001901.

Coates, A. G., and R. F. Stallard (2013), How old is the Isthmus of Panama?, *Bull. Mar. Sci.*, *89*(4), 801–813, doi:10.5343/bms.2012.1076.

Cristini, L., K. Grosfeld, M. Butzin, and G. Lohmann (2012), Influence of the opening of the Drake Passage on the Cenozoic Antarctic ice sheet: A modeling approach, *Palaeogeogr. Palaeoclimatol. Palaeoecol.*, *339–341*, 66–73, doi:10.1016/j.palaeo.2012.04.023.

Cunningham, S. A., S. G. Alderson, B. A. King, and M. A. Brandon (2003), Transport and variability of the Antarctic circumpolar current in Drake Passage, *J. Geophys. Res.*, *108*(C5), 8084, doi:10.1029/2001JC001147.

DeConto, R. M., and D. Pollard (2003a), Rapid Cenozoic glaciation of Antarctica induced by declining atmospheric CO_2, *Nature*, *421*(6920), 245–249, doi:10.1038/nature01290.

DeConto, R. M., and D. Pollard (2003b), A coupled climate-ice sheet modeling approach to the early Cenozoic history of the Antarctic ice sheet, *Palaeogeogr. Palaeoclimatol. Palaeoecol.*, *198*(1–2), 39–52, doi:10.1016/S0031-0182(03)00393-6.

Eagles, G., R. Livermore, and P. Morris (2006), Small basins in the Scotia Sea: The Eocene Drake Passage Gateway, *Earth Planet. Sci. Lett.*, *242*(3–4), 343–353, doi:10.1016/j.epsl.2005.11.060.

Frank, M. (2002), Radiogenic isotopes: Tracers of past ocean circulation and erosional input, *Rev. Geophys.*, *40*(1), 1–38, doi:10.1029/2000RG000094.

Frank, M., B. C. Reynolds, and K. R. O'Nions (1999), Nd and Pb isotopes in Atlantic and Pacific water masses before and after closure of the Panama Gateway, *Geology*, *27*(12), 1147–1150, doi:10.1130/0091-7613(1999)027<1147:NAPIIA>2.3.CO;2.

Frank, M., N. Whiteley, S. Kasten, J. R. Hein, and K. O'Nions (2002), North Atlantic deep water export to the Southern Ocean over the past 14 Myr: Evidence from Nd and Pb isotopes in ferromanganese crusts, *Paleoceanography*, *17*(2), 1022, doi:10.1029/2000PA000606.

Gerber, M., and F. Joos (2013), An ensemble Kalman filter multi-tracer assimilation: Determining uncertain ocean model parameters for improved climate-carbon cycle projections, *Ocean Model.*, *64*, 29–45, doi:10.1016/j.ocemod.2012.12.012.

Gill, A. E., and K. Bryan (1971), Effects of geometry on the circulation of a three-dimensional Southern-Hemisphere ocean model, *Deep Sea Res. Oceanogr. Abstr.*, *18*(7), 685–721, doi:10.1016/0011-7471(71)90086-6.

Goldner, A., N. Herold, and M. Huber (2014), Antarctic glaciation caused ocean circulation changes at the Eocene-Oligocene transition, *Nature*, *511*(7511), 574–577, doi:10.1038/nature13597.

Heinemann, M. (2009), Warm and sensitive Paleocene-Eocene climate, PhD thesis, Dept. Geowissenschaften der Univ. Hamburg, Hamburg, Germany. [Available at http://www.mpimet.mpg.de/fileadmin/publikationen/Reports/WEB_BzE_70.pdf.]

Huber, M., and D. Nof (2006), The ocean circulation in the Southern Hemisphere and its climatic impacts in the Eocene, *Palaeogeogr. Palaeoclimatol. Palaeoecol.*, *231*(1–2), 9–28, doi:10.1016/j.palaeo.2005.07.037.

Huber, M., and L. C. Sloan (2001), Heat transport, deep waters, and thermal gradients: Coupled simulation of an Eocene greenhouse climate, *Geophys. Res. Lett.*, *28*(18), 3481–3484, doi:10.1029/2001GL012943.

Jacobsen, S. B., and G. Wasserburg (1980), Sm-Nd isotopic evolution of chondrites, *Earth Planet. Sci. Lett.*, *50*(1), 139–155, doi:10.1016/0012-821X(80)90125-9.

Jeandel, C., T. Arsouze, F. Lacan, P. Téchiné, and J.-C. Dutay (2007), Isotopic Nd compositions and concentrations of the lithogenic inputs into the ocean: A compilation, with an emphasis on the margins, *Chem. Geol.*, *239*(1–2), 156–164, doi:10.1016/j.chemgeo.2006.11.013.

Kennett, J. P. (1977), Cenozoic evolution of Antarctic glaciation, the circum-Antarctic Ocean, and their impact on global paleoceanography, *J. Geophys. Res.*, *82*(27), 3843–3860, doi:10.1029/JC082i027p03843.

Klocker, A., M. Prange, and M. Schulz (2005), Testing the influence of the Central American Seaway on orbitally forced Northern Hemisphere glaciation, *Geophys. Res. Lett.*, *32*, L03703, doi:10.1029/2004GL021564.

Lacan, F., and C. Jeandel (2005), Neodymium isotopes as a new tool for quantifying exchange fluxes at the continent—Ocean interface, *Earth Planet. Sci. Lett.*, *232*(3–4), 245–257, doi:10.1016/j.epsl.2005.01.004.

Lefebvre, V., Y. Donnadieu, P. Sepulchre, D. Swingedouw, and Z.-S. Zhang (2012), Deciphering the role of southern gateways and carbon dioxide on the onset of the Antarctic circumpolar current, *Paleoceanography*, *27*, PA4201, doi:10.1029/2012PA002345.

Livermore, R., A. Nankivell, G. Eagles, and P. Morris (2005), Paleogene opening of Drake Passage, *Earth Planet. Sci. Lett.*, *236*(1–2), 459–470, doi:10.1016/j.epsl.2005.03.027.

Lunt, D. J., P. J. Valdes, A. Haywood, and I. C. Rutt (2008), Closure of the Panama Seaway during the Pliocene: Implications for climate and Northern Hemisphere glaciation, *Clim. Dyn.*, *30*(1), 1–18, doi:10.1007/s00382-007-0265-6.

Lunt, D. J., P. J. Valdes, T. Dunkley Jones, A. Ridgwell, A. M. Haywood, D. N. Schmidt, R. Marsh, and M. Maslin (2010), CO_2-driven ocean circulation changes as an amplifier of Paleocene-Eocene thermal maximum hydrate destabilization, *Geology*, *38*(10), 875–878, doi:10.1130/G31184.1.

Maier-Reimer, E., U. Mikolajewicz, and T. J. Crowley (1990), Ocean general circulation model sensitivity experiment with an open central American Isthmus, *Paleoceanography*, *5*(3), 349–366, doi:10.1029/PA005i003p00349.

Menviel, L., F. Joos, and S. Ritz (2012), Simulating atmospheric CO_2, ^{13}C and the marine carbon cycle during the last glacial-interglacial cycle: Possible role for a deepening of the mean remineralization depth and an increase in the oceanic nutrient inventory, *Quat. Sci. Rev.*, *56*, 46–68, doi:10.1016/j.quascirev.2012.09.012.

Mikolajewicz, U., E. Maier-Reimer, T. J. Crowley, and K. Y. Kim (1993), Effect of Drake and Panamanian Gateways on the circulation of an ocean model, *Paleoceanography*, *8*(4), 409–426, doi:10.1029/93PA00893.

Molnar, P. (2008), Closing of the Central American seaway and the ice age: A critical review, *Paleoceanography*, *23*, PA2201, doi:10.1029/2007PA001574.

Montes, C., et al. (2012a), Evidence for middle Eocene and younger land emergence in central Panama: Implications for Isthmus closure, *Geol. Soc. Am. Bull.*, *124*(5–6), 780–799, doi:10.1130/B30528.1.

Montes, C., G. Bayona, A. Cardona, D. M. Buchs, C. A. Silva, S. Morón, N. Hoyos, D. A. Ramírez, C. A. Jaramillo, and V. Valencia (2012b), Arc-continent collision and orocline formation: Closing of the Central American Seaway, *J. Geophys. Res.*, *117*, B04105, doi:10.1029/2011JB008959.

Motoi, T., W.-L. Chan, S. Minobe, and H. Sumata (2005), North Pacific halocline and cold climate induced by Panamanian Gateway closure in a coupled ocean-atmosphere GCM, *Geophys. Res. Lett.*, *32*, L10618, doi:10.1029/2005GL022844.

Muiños, S. B., M. Frank, C. Maden, J. R. Hein, T. van de Flierdt, S. M. Lebreiro, L. Gaspar, J. H. Monteiro, and A. N. Halliday (2008), New constraints on the Pb and Nd isotopic evolution of NE Atlantic water masses, *Geochem. Geophys. Geosyst.*, *9*, Q02007, doi:10.1029/2007GC001766.

Müller, S. A., F. Joos, N. R. Edwards, and T. F. Stocker (2006), Water mass distribution and ventilation time scales in a cost-efficient, three-dimensional ocean model, *J. Clim.*, *19*(21), 5479–5499, doi:10.1175/JCLI3911.1.

Murdock, T. Q., A. J. Weaver, and A. F. Fanning (1997), Paleoclimatic response of the closing of the Isthmus of Panama in a coupled ocean-atmosphere model, *Geophys. Res. Lett.*, *24*(3), 253–256, doi:10.1029/96GL03950.

Newkirk, D. R., and E. E. Martin (2009), Circulation through the Central American Seaway during the Miocene carbonate crash, *Geology*, *37*(1), 87–90, doi:10.1130/G25193A.1.

Nisancioglu, K. H., M. E. Raymo, and P. H. Stone (2003), Reorganization of Miocene deep water circulation in response to the shoaling of the Central American Seaway, *Paleoceanography*, *18*(1), 1006, doi:10.1029/2002PA000767.

O'Nions, R. K., M. Frank, F. von Blanckenburg, and H.-F. Ling (1998), Secular variation of Nd and Pb isotopes in ferromanganese crusts from the Atlantic, Indian and Pacific Oceans, *Earth Planet. Sci. Lett.*, *155*(1–2), 15–28, doi:10.1016/S0012-821X(97)00207-0.

Osborne, A. H., B. A. Haley, E. C. Hathorne, S. Flögel, and M. Frank (2014), Neodymium isotopes and concentrations in Caribbean seawater: Tracing water mass mixing and continental input in a semi-enclosed ocean basin, *Earth Planet. Sci. Lett.*, *406*, 174–186, doi:10.1016/j.epsl.2014.09.011.

Parekh, P., F. Joos, and S. A. Müller (2008), A modeling assessment of the interplay between aeolian iron fluxes and iron-binding ligands in controlling carbon dioxide fluctuations during Antarctic warm events, *Paleoceanography*, *23*, PA4202, doi:10.1029/2007PA001531.

Poore, H. R., R. Samworth, N. J. White, S. M. Jones, and I. N. McCave (2006), Neogene overflow of northern component water at the Greenland-Scotland Ridge, *Geochem. Geophys. Geosyst.*, *7*, Q06010, doi:10.1029/2005GC001085.

Rempfer, J., T. F. Stocker, F. Joos, J. Dutay, and M. Siddall (2011), Modelling Nd-isotopes with a coarse resolution ocean circulation model: Sensitivities to model parameters and source/sink distributions, *Geochim. Cosmochim. Acta*, *75*(20), 5927–5950, doi:10.1016/j.gca.2011.07.044.

Rempfer, J., T. F. Stocker, F. Joos, and J. Dutay (2012a), On the relationship between Nd isotopic composition and ocean overturning circulation in idealized freshwater discharge events, *Paleoceanography*, *27*, PA3211, doi:10.1029/2012PA002312.

Rempfer, J., T. F. Stocker, F. Joos, and J.-C. Dutay (2012b), Sensitivity of Nd isotopic composition in seawater to changes in Nd sources and paleoceanographic implications, *J. Geophys. Res.*, *117*, C12010, doi:10.1029/2012JC008161.

Reynolds, B., M. Frank, and R. O'Nions (1999), Nd- and Pb-isotope time series from Atlantic ferromanganese crusts: Implications for changes in provenance and paleocirculation over the last 8 Myr, *Earth Planet. Sci. Lett.*, *173*(4), 381–396, doi:10.1016/S0012-821X(99)00243-5.

Ritz, S. P., T. F. Stocker, and F. Joos (2011), A coupled dynamical ocean-energy balance atmosphere model for paleoclimate studies, *J. Clim.*, *24*(2), 349–375, doi:10.1175/2010JCLI3351.1.

Ritz, S. P., T. F. Stocker, J. O. Grimalt, L. Menviel, and A. Timmermann (2013), Estimated strength of the Atlantic overturning circulation during the last deglaciation, *Nat. Geosci.*, *6*(3), 208–212, doi:10.1038/ngeo1723.

Roth, R., and F. Joos (2013), A reconstruction of radiocarbon production and total solar irradiance from the Holocene ^{14}C and CO_2 records: Implications of data and model uncertainties, *Clim. Past*, *9*(4), 1879–1909, doi:10.5194/cp-9-1879-2013.

Scher, H. D., and E. E. Martin (2004), Circulation in the Southern Ocean during the Paleogene inferred from neodymium isotopes, *Earth Planet. Sci. Lett.*, *228*(3–4), 391–405, doi:10.1016/j.epsl.2004.10.016.

Scher, H. D., and E. E. Martin (2006), Timing and climatic consequences of the opening of Drake Passage, *Science*, *312*(5772), 428–430, doi:10.1126/science.1120044.

Scher, H. D., and E. E. Martin (2008), Oligocene deep water export from the North Atlantic and the development of the Antarctic Circumpolar Current examined with neodymium isotopes, *Paleoceanography*, *23*, PA1205, doi:10.1029/2006PA001400.

Schneider, B., and A. Schmittner (2006), Simulating the impact of the Panamanian Seaway closure on ocean circulation, marine productivity and nutrient cycling, *Earth Planet. Sci. Lett.*, *246*(3–4), 367–380, doi:10.1016/j.epsl.2006.04.028.

Sepulchre, P., T. Arsouze, Y. Donnadieu, J.-C. Dutay, C. Jaramillo, J. Le Bras, E. Martin, C. Montes, and A. J. Waite (2014), Consequences of shoaling of the Central American Seaway determined from modeling Nd isotopes, *Paleoceanography*, *29*, 176–189, doi:10.1002/2013PA002501.

Sijp, W. P., and M. H. England (2004), Effect of the Drake Passage throughflow on global climate, *J. Phys. Oceanogr.*, *34*(5), 1254–1266, doi:10.1175/1520-0485(2004)034<254:EOTDPT>2.0.CO;2.

Sijp, W. P., M. H. England, and J. R. Toggweiler (2009), Effect of ocean gateway changes under greenhouse warmth, *J. Clim.*, *22*(24), 6639–6652, doi:10.1175/2009JCLI3003.1.

Sijp, W. P., M. H. England, and M. Huber (2011), Effect of the deepening of the Tasman Gateway on the global ocean, *Paleoceanography*, *26*, PA4207, doi:10.1029/2011PA002143.

Smith, R. S., C. Dubois, and J. Marotzke (2006), Global climate and ocean circulation on an aquaplanet ocean-atmosphere general circulation model, *J. Clim.*, *19*(18), 4719–4737, doi:10.1175/JCLI3874.1.

Steph, S., R. Tiedemann, M. Prange, J. Groeneveld, M. Schulz, A. Timmermann, D. Nürnberg, C. Rühlemann, C. Saukel, and G. H. Haug (2010), Early Pliocene increase in thermohaline overturning: A precondition for the development of the modern equatorial Pacific cold tongue, *Paleoceanography*, *25*, PA2202, doi:10.1029/2008PA001645.

Stichel, T., M. Frank, J. Rickli, and B. A. Haley (2012), The hafnium and neodymium isotope composition of seawater in the Atlantic sector of the Southern Ocean, *Earth Planet. Sci. Lett.*, *317–318*, 282–294, doi:10.1016/j.epsl.2011.11.025.

Stocker, T. F., A. Timmermann, M. Renold, and O. Timm (2007), Effects of salt compensation on the climate model response in simulations of large changes of the Atlantic meridional overturning circulation, *J. Clim.*, *20*(24), 5912–5928, doi:10.1175/2007JCLI1662.1.

Stone, R. (2013), Battle for the Americas, *Science*, *341*(6143), 230–233, doi:10.1126/science.341.6143.230.

Toggweiler, J. R., and H. Bjornsson (2000), Drake Passage and palaeoclimate, *J. Quat. Sci.*, *15*(4), 319–328, doi:10.1002/1099-1417(200005)15:4<319::AID-JQS545>3.0.CO;2-C.

Toggweiler, J. R., and B. Samuels (1995), Effect of Drake Passage on the global thermohaline circulation, *Deep Sea Res. Part I*, *42*(4), 477–500, doi:10.1016/0967-0637(95)00012-U.

Tschumi, T., F. Joos, and P. Parekh (2008), How important are Southern Hemisphere wind changes for low glacial carbon dioxide? A model study, *Paleoceanography*, *23*, PA4208, doi:10.1029/2008PA001592.

von Blanckenburg, F., and T. Nägler (2001), Weathering versus circulation-controlled changes in radiogenic isotope tracer composition of the Labrador Sea and North Atlantic Deep Water, *Paleoceanography*, *16*(4), 424–434, doi:10.1029/2000PA000550.

von der Heydt, A., and H. A. Dijkstra (2006), Effect of ocean gateways on the global ocean circulation in the late Oligocene and early Miocene, *Paleoceanography*, *21*, PA1011, doi:10.1029/2005PA001149.

Zaucker, F., T. F. Stocker, and W. S. Broecker (1994), Atmospheric fresh-water fluxes and their effect on the global thermohaline circulation, *J. Geophys. Res.*, *99*(C6), 12,443–12,457, doi:10.1029/94JC00526.

Zhang, X., et al. (2012), Changes in equatorial Pacific thermocline depth in response to Panamanian Seaway closure: Insights from a multi-model study, *Earth Planet. Sci. Lett.*, *317–318*, 76–84, doi:10.1016/j.epsl.2011.11.028.

Zhang, Z.-S., Q. Yan, and H.-J. Wang (2010), Has the Drake Passage played an essential role in the Cenozoic cooling?, *Atmos. Oceanic Sci. Lett.*, *3*(5), 288–292.